Article

Current Biology

Sharper, Stronger, Faster Upper Visual Field Representation in Primate Superior Colliculus

Highlights

- Smaller upper visual field SC visual and saccade-related response fields
- Higher spatial-frequency tuning and contrast sensitivity in the upper visual field
- Over-representation of the upper visual field in visual and saccade-related SC maps
- SC tuning to smaller image features typically encountered in upper visual fields

Authors

Ziad M. Hafed, Chih-Yang Chen

Correspondence

ziad.m.hafed@cin.uni-tuebingen.de

In Brief

Hafed and Chen show that the superior colliculus (SC) contains a functional discontinuity in spatial resolution and neural sensitivity between upper (UVF) and lower (LVF) visual field representations. This recasts prior knowledge of SC topography, assuming UVF/LVF symmetry, and demonstrates how the SC can support more accurate, lower-latency UVF saccades.

Hafed & Chen, 2016, Current Biology *26*, 1647–1658
July 11, 2016
http://dx.doi.org/10.1016/j.cub.2016.04.059

CellPress

Current Biology
Article

Sharper, Stronger, Faster Upper Visual Field Representation in Primate Superior Colliculus

Ziad M. Hafed[1,*] and Chih-Yang Chen[1,2]
[1]Werner Reichardt Centre for Integrative Neuroscience, Tuebingen University, Tuebingen BW 72076, Germany
[2]Graduate School of Neural and Behavioural Sciences, International Max Planck Research School, Tuebingen University, Tuebingen BW 72074, Germany
*Correspondence: ziad.m.hafed@cin.uni-tuebingen.de
http://dx.doi.org/10.1016/j.cub.2016.04.059

SUMMARY

Visually guided behavior in three-dimensional environments entails handling immensely different sensory and motor conditions across retinotopic visual field locations: peri-personal ("near") space is predominantly viewed through the lower retinotopic visual field (LVF), whereas extra-personal ("far") space encompasses the upper visual field (UVF). Thus, when, say, driving a car, orienting toward the instrument cluster below eye level is different from scanning an upcoming intersection, even with similarly sized eye movements. However, an overwhelming assumption about visuomotor circuits for eye-movement exploration, like those in the primate superior colliculus (SC), is that they represent visual space in a purely symmetric fashion across the horizontal meridian. Motivated by ecological constraints on visual exploration of far space, containing small UVF retinal-image features, here we found a large, multi-faceted difference in the SC's representation of the UVF versus LVF. Receptive fields are smaller, more finely tuned to image spatial structure, and more sensitive to image contrast for neurons representing the UVF. Stronger UVF responses also occur faster. Analysis of putative synaptic activity revealed a particularly categorical change when the horizontal meridian is crossed, and our observations correctly predicted novel eye-movement effects. Despite its appearance as a continuous layered sheet of neural tissue, the SC contains functional discontinuities between UVF and LVF representations, paralleling a physical discontinuity present in cortical visual areas. Our results motivate the recasting of structure-function relationships in the visual system from an ecological perspective, and also exemplify strong coherence between brain-circuit organization for visually guided exploration and the nature of the three-dimensional environment in which we function.

INTRODUCTION

The primate superior colliculus (SC) is a layered midbrain structure critical for visual-motor processing, target selection, and attention [1–11], and it is particularly important for sensorimotor transformations from retinal image features into gaze shift commands [5–7, 12]. Superficial SC layers contain retinotopic maps of the contralateral visual field, and deeper layers contain spatially registered eye-movement maps [13–15]. Visual, visual-motor, and motor neurons possess response fields (RFs) confined to a region of visual (afferent) or movement (efferent) space, and RF sizes are often large. This means that the SC may use coarse population coding to ensure accurate localization [16–19].

Much like primary visual cortex, the SC magnifies foveal representations [13, 14]. Such magnification affords smaller and more abundant RFs dedicated to processing small retinotopic eccentricities [13], which increases spatial resolution [16]. Indeed, RFs associated with microsaccades, which precisely relocate gaze on a miniature scale [20, 21], are smaller than peripheral RFs associated with large saccades [22, 23]. Observations like these have led to a universally accepted model [19] in which retinotopic eccentricity morphs onto SC tissue using logarithmic warping. In this model, more tissue represents central locations, and with higher resolution, but upper (UVF) and lower (LVF) visual field representations are identical.

However, our environment dictates different constraints on eye-movement exploration between the UVF and LVFs [24]. For example, the LVF encompasses peri-personal "near" space, in which objects project larger retinal images, whereas UVF objects are generally "far" and project small features (Figures 1A and S1A) [24]. In this study, we hypothesized that SC organization might be "in tune" with such ecological constraints on eye-movement exploration [24]. We discovered a significant asymmetry across the horizontal meridian, spanning both anatomical mapping as well as physiological and behavioral properties. This asymmetry is such that SC visual-motor processing allows more accurate and lower-latency saccades to UVF image features.

We will show, among other things, that UVF SC RFs are smaller than LVF RFs. This suggests UVF magnification in neural tissue, similar in principle to foveal magnification. We will thus propose a revised model more accurately representing SC topography than the universally accepted model [14, 19]. Our revised understanding of SC topography is not only in line with behavioral effects, but it may also be a critical missing link for resolving some long-standing debates about SC saccade-related dynamics [9, 25–27]. More broadly, our results motivate recasting of structure-function relationships in the visual system from an ecological perspective [24]. This sentiment is contrary to common practice. For example, because dorsal cortex (primarily

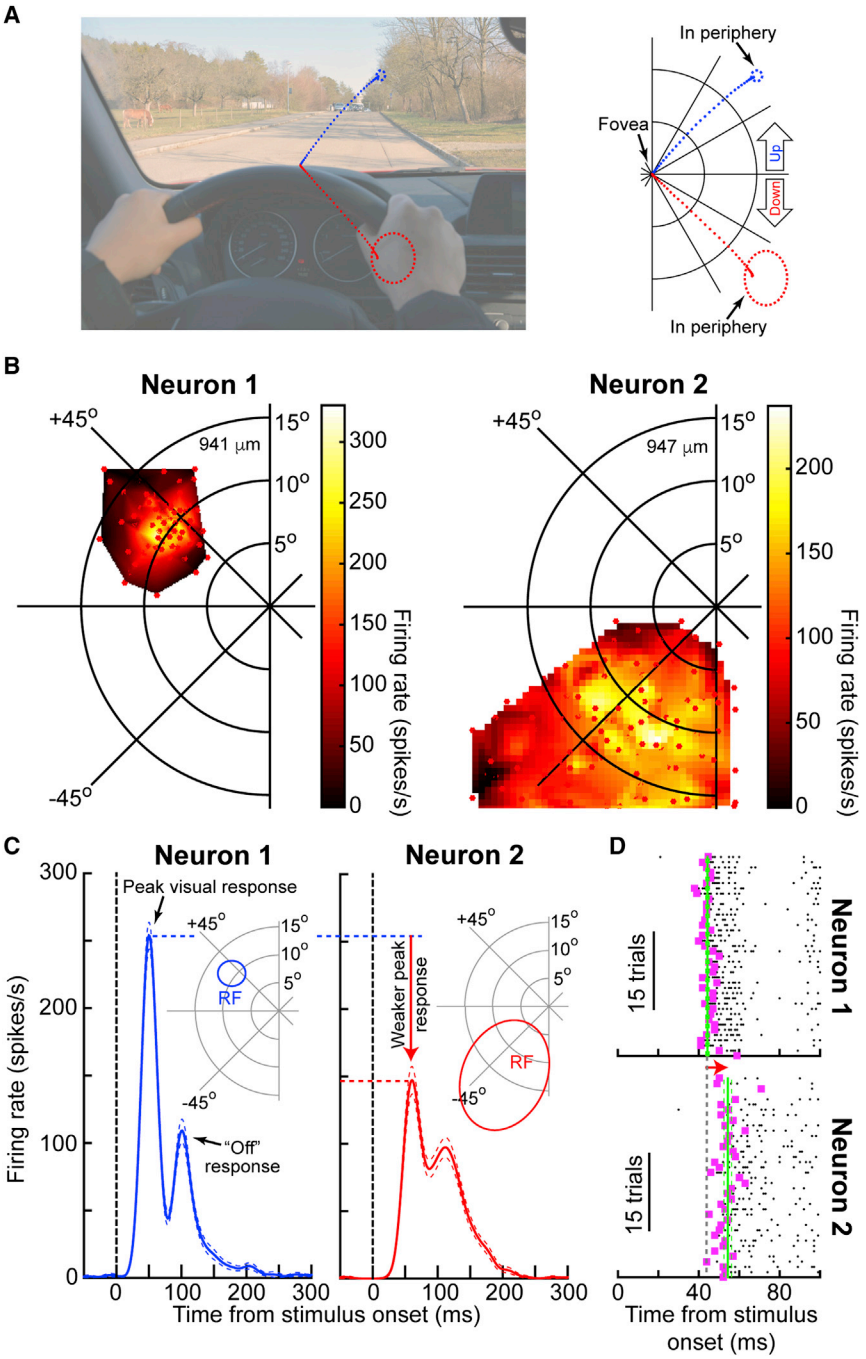

Figure 1. Sharper, Stronger, Faster UVF SC Representation

(A) In retinotopic coordinates, UVF features are generally farther and smaller than LVF features [24]. In this example, a driver initially looks down near the instrument cluster. A bird on a treetop might attract his gaze, requiring an upward saccade; a similarly sized saccade can be made to the LVF (if, for example, something itches on his hand). The spatial scales at the ends of the two, otherwise identical, saccades differ (dashed circles). Also see Figure S1A.

(B) Visual RFs from two example visual neurons (the depth from the SC surface is indicated in each panel). Individual dots show sampled stimulus locations. The neurons were matched for animal, side of space, depth, and hotspot eccentricity (i.e., eccentricity of peak response), but the UVF RF was smaller.

(C) Firing rates of the same neurons for a flashed spot at the preferred RF hotspot. The UVF neuron had a stronger response (measured as the peak response within 30–150 ms after stimulus onset). Note that the neurons showed a later "off" response because of the brief stimulus flash. Error bars, which are indicated by thin dashed lines around the data curves, indicate the SEM.

(D) The same visual responses but shown as spike rasters. Each dot is a spike; each row is a trial. The first stimulus-evoked spike is magenta, and green vertical lines indicate the mean/SEM first-spike latency. Visual responses occurred faster for the UVF neuron. The arrow indicates the time difference between the mean latency of neuron 1 and the mean latency of neuron 2

Also see Figure S1.

representing the LVF) is more readily accessible experimentally, there exists a strong bias to study only the LVF. Such bias might mask interesting UVF versus LVF dissociations [24].

RESULTS

We recorded from 419 neurons (157 visual, 251 visual-motor, and 11 motor) in two monkeys performing visual and saccade-related tasks (Experimental Procedures). We analyzed visual and saccade-related activity as well as RF properties. Our database spanned a range of eccentricities and directions (Figures S1B–S1E) and was balanced, with 52.21% of neurons preferring UVF RF locations and 47.79% preferring LVF locations.

We observed a large change in visual RF area as a function of visual field location. Figure 1B shows RFs from two example visual neurons recorded from the same SC side, same animal, same electrode depth from the SC surface, and, most importantly, same RF hotspot eccentricity (defined as the stimulus location giving maximal visual response). In each panel, we plotted visual burst strength as a function of stimulus location from a delayed visually guided saccade task used to map RFs (Experimental Procedures). The figure shows locations with significant visual responses above each neuron's no-stimulus baseline (Experimental Procedures). The UVF RF (neuron 1) was ~76% smaller than the LVF RF (neuron 2) (60.43 degrees^2 versus 251 degrees^2).

This effect was accompanied by stronger and lower-latency responses. For the same neurons, we analyzed visual responses when the monkeys fixated, and we presented a briefly flashed spot at each neuron's preferred hotspot (Experimental

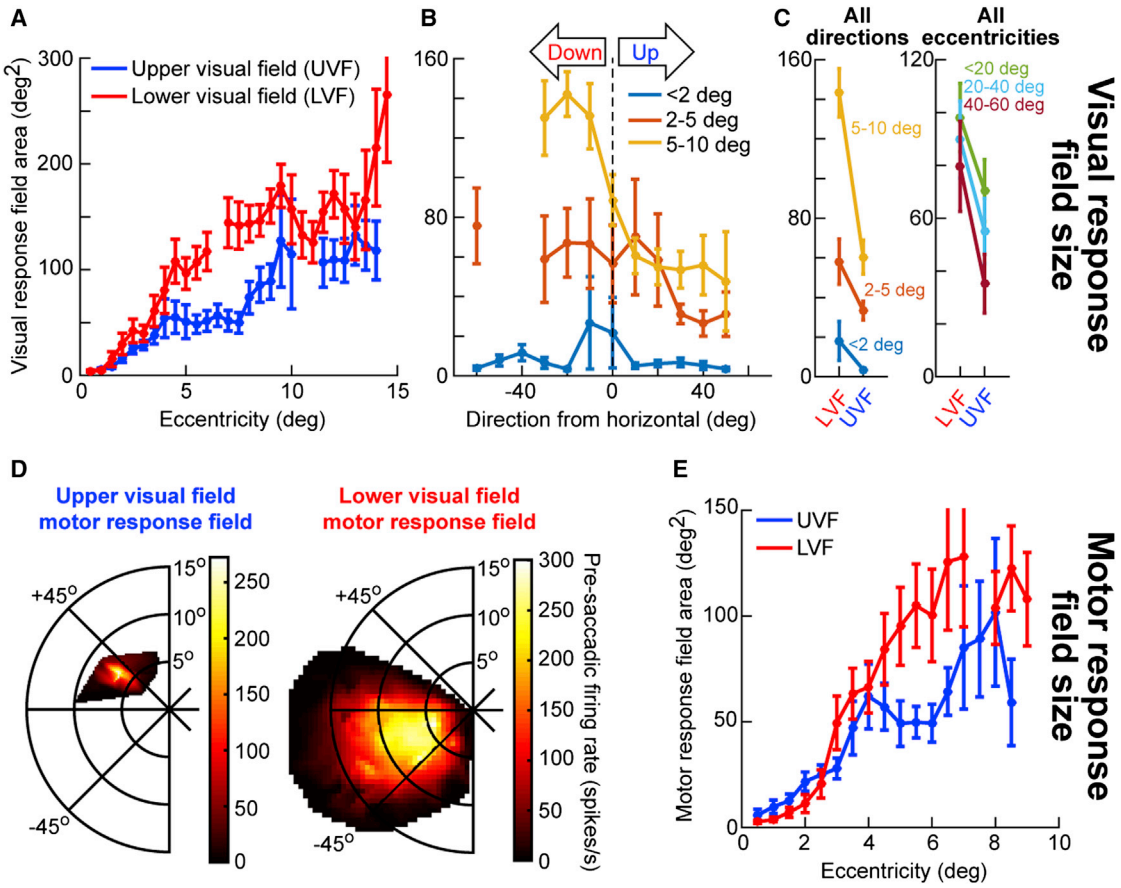

Figure 2. Higher-Resolution UVF Spatial Representation

(A) Visual RF area (Experimental Procedures) increased with eccentricity [13], but more dramatically for LVF neurons.

(B) Same data as in (A), but as a function of RF direction from horizontal.

(C) Same data, but collapsing across directions or eccentricities.

(D) Example eccentricity-matched motor RFs showing a similar asymmetry. All conventions are similar to Figure 1B, but here we measured pre-saccadic (0–50 ms before saccade onset) firing rate.

(E) Like (A), but for motor RFs.

Error bars indicate the SEM. Also see Figures S2–S4.

Procedures). We measured peak response 30–150 ms after stimulus onset and found that the UVF neuron had ~1.66 times the response of the LVF neuron (Figure 1C; $p < 0.05$, two-tailed t test). Moreover, latency to first stimulus-induced spike was lower (Figure 1D; $p < 0.05$, two-tailed t test). Thus, UVF SC representations have smaller RFs and stronger, lower-latency visual responses.

We next describe the robustness of these findings, their relation to motor RF properties, as well as their implications for behavioral properties of saccades and SC topographic representations.

Higher-Resolution Coverage of the Upper Visual Field

We plotted visual RF area (Experimental Procedures) as a function of hotspot eccentricity (Figure 2A). RF area increased with eccentricity [13], but the increase was stronger for LVF RFs (two-way ANOVA, $p < 0.05$ for both main effects of eccentricity and UVF/LVF location). We also analyzed RF area as a function of direction from horizontal (Figure 2B): both direction and eccentricity had an impact (two-way ANOVA, $p < 0.05$ for both main effects of eccentricity and direction). The same conclusion was reached when collapsing across directions (Figure 2C, left; two-way ANOVA, $p < 0.05$); moreover, for individual eccentricity bins, 2- to 5-degree and 5- to 10-degree eccentricities each had larger LVF RFs than UVF RFs ($p < 0.05$, two-tailed t tests; Figure 2C, left). The effect was weakest for foveal eccentricities, for which RF sizes are already small. Similar analyses when collapsing across eccentricities (Figure 2C, right) also revealed a main effect of UVF/LVF location ($p < 0.05$, two-way ANOVA). However, this time, there was no main effect of direction ($p > 0.05$), suggestive of a categorical change across the horizon (i.e., even directions <20 degrees showed an area difference between UVF and LVF).

Because RF area increases with depth from the SC surface [28], we also confined analyses to the most superficial layers (<1 mm below the surface [8]) and still observed UVF/LVF differences (Figure S2A). Thus, Figures 2A–2C are not an artifact of combining different depths. We also found similar UVF/LVF

asymmetries in either right or left SC individually (Figure S2B). Moreover, for neurons with predominantly vertical RF hotspots, LVF RFs were uncharacteristically elongated, almost forming an edge-like representation (Figure S2C). Finally, for deeper visual-motor and motor neurons, even UVF saccade-related motor RFs were smaller. This is illustrated in Figure 2D for two eccentricity-matched visual-motor neurons recorded during the same delayed visually guided saccade task as that in Figure 1B. Pre-saccadic firing rate was plotted as a function of saccade endpoint (Experimental Procedures), and the LVF neuron still had a larger motor RF; this was also consistent across the population (Figures 2E and S3; two-way ANOVA, $p < 0.05$ for both main effects of eccentricity and UVF/LVF location).

Therefore, even when separately analyzing different depths, individual SCs, and saccade-related RFs, UVF/LVF RF area differences persisted and extended to efferent representations.

With larger LVF RFs, a given stimulus or saccade endpoint would activate neurons with RF hotspots at significantly more retinotopic locations than a similarly eccentric UVF stimulus. We confirmed this for visual (Figure S4A) and saccade-related (Figure S4B) representations. Such a difference in spatial pooling is reminiscent of psychophysical differences in illusory contour integration between the UVF and LVFs [29].

Higher Spatial-Frequency Tuning and Contrast Sensitivity in the Upper Visual Field

Another implication of a sharper UVF spatial representation (i.e., with smaller RFs) is that it might extend to other aspects of spatial vision. We hypothesized that sensitivity to fine spatial structure might be higher in the SC's UVF representation. We therefore characterized SC spatial-frequency tuning properties (Experimental Procedures). The monkeys fixated while we presented a stationary grating within an RF. We observed individual preferences for individual spatial frequencies (Figure 3A). Like in primary visual cortex [30, 31], individual eccentricities had neurons representing multiple spatial frequencies, and tuning curves became increasingly low pass eccentrically (Figure S5). Remarkably, beyond the parafovea, UVF neurons exhibited more tuning to higher spatial frequencies (Figures 3A and 3B). Thus, the existence of multiple spatial-frequency channels at a given eccentricity persists farther out in the periphery for UVF representations. We statistically confirmed this by testing for a larger UVF dispersion of preferred frequencies (Figure 3B; $p < 0.05$, median-subtracted Ansari-Bradley test for dispersions).

We also tested contrast sensitivity using the task of [32]. Once again, UVF neurons had higher sensitivity (i.e., lower semi-saturation contrasts; $p < 0.05$, two-tailed t test) and larger dynamic range ($p < 0.05$, two-tailed t test) (Figures 3C and 3D). Thus, UVF SC visual RFs are smaller, more finely tuned to spatial structure, and more sensitive to image contrast.

Stronger, Lower-Latency Upper Visual Field Visual Responses

We explored the increased sensitivity property further by analyzing visual response strength for a briefly flashed spot at the RF hotspot while the monkeys fixated (from the same task used in Figure 1C; Experimental Procedures). Peak UVF responses were ~1.33 times stronger than peak LVF responses (Figure 4A; $p < 0.05$, two-tailed t test), and this effect persisted for different directions from horizontal (Figures 4B and 4C; $p < 0.05$, one-way ANOVA with direction as the main factor). Like in the example neurons (Figure 1), we also confirmed that UVF neurons also exhibited lower visual response latencies (Figures 4D and 4E; $p < 0.05$, two-tailed t test; also demonstrated in Figure 4F; $p < 0.05$, one-way ANOVA with direction as the main factor). Given that SC visual bursts strongly correlate with saccadic reaction times (RTs) [33–35], these observations (Figures 4A–4F) help explain previously reported decreases in UVF visually guided saccade RTs [36, 37]. Such effects, which we replicated (Figure S6A, left panel; Figure S6B, leftmost panel), have eluded a neurobiologically plausible mechanism for several decades [24].

Interestingly, stronger UVF activity was specific for visual responses. Saccade-related activity showed the opposite effect: across directions, pre-saccadic activity was weaker in the UVF (Figure 4G; $p < 0.05$, two-tailed t test), and there was a direction main effect (Figures 4H and 4I; $p < 0.05$, one-way ANOVA). Thus, in the UVF, it is visual SC modulations that are particularly strong.

Given that the SC receives inputs from several cortical visual areas [38], in which there is a physical discontinuity between UVF and LVF representations [39, 40], we hypothesized that an SC functional discontinuity in visual representations might parallel a cortical structural discontinuity. We analyzed visually evoked local field potentials (LFPs) as a proxy for aggregate synaptic activity after stimulus onset (Experimental Procedures). We did this for the same task for which we analyzed visually evoked spiking (Figures 1C, 1D, and 4A–4F). An even stronger UVF asymmetry emerged: across eccentricities, stimulus-evoked LFP modulation was ~2.5 times stronger for UVF RFs compared to LVF RFs (Figure 5A; $p < 0.05$, two-tailed t test). Additionally, there was a categorical change in response strength across the horizontal meridian (Figure 5B): for all UVF direction bins, LFP response was much stronger than for all LVF bins, and the effect was approximately equal for different directions (Figures 5B–5D) and eccentricities (Figures 5D and 5E). We confirmed this statistically: two-way ANOVAs with UVF/LVF location as one factor and eccentricity or direction as the other revealed a main effect of only UVF/LVF location ($p < 0.05$). This suggests a categorical change, or functional discontinuity, across the horizontal meridian.

Lower-Latency, More Accurate Upper Visual Field Saccades

Using visually guided saccades (Experimental Procedures), we confirmed that UVF saccades are not only lower latency (as stated above) but also more accurate (Figure S6A; Figure S6B, two leftmost panels). The RT effect is likely a consequence of visual response effects (Figures 4 and 5), and the accuracy effect probably reflects smaller UVF motor RFs (Figures 2D, 2E, and S3).

Using visually guided saccades, we also discovered that express saccades (with RTs <100 ms) [41] were 9–14 times more likely for UVF rather than LVF targets (Figure S6B, rightmost panel). This large effect is surprising given that express saccades should be rare (if not absent) in this task [41].

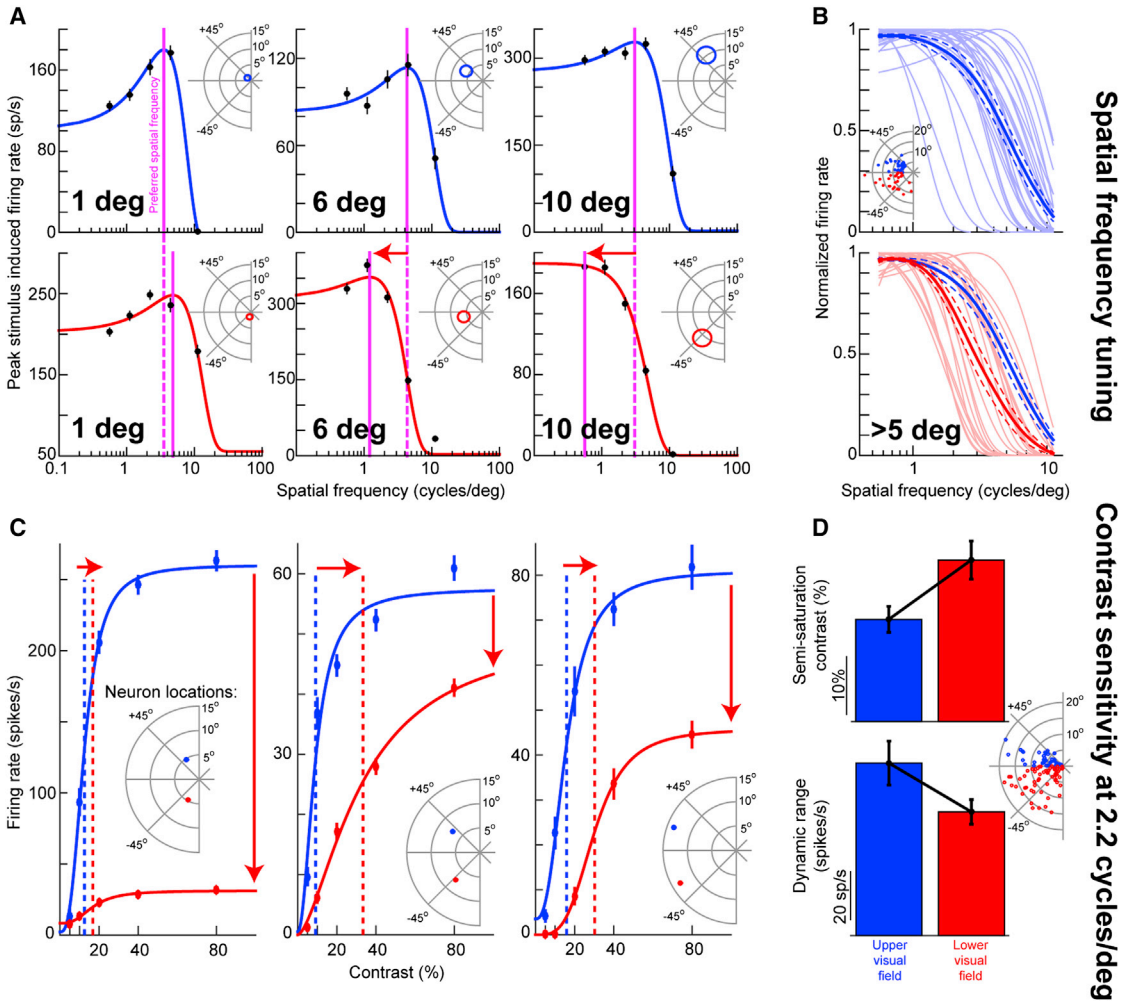

Figure 3. Higher UVF Spatial-Frequency Tuning and Contrast Sensitivity

(A) Sample spatial-frequency tuning curves for three eccentricity-matched pairs of UVF/LVF neurons. Each column shows one eccentricity, and the top and bottom rows show UVF and LVF neurons, respectively. UVF eccentric neurons (6 and 10 degrees) had higher preferred spatial frequency (magenta lines) than LVF neurons. The insets show neuron locations.

(B) Normalized tuning curves for all eccentric neurons (>5 degrees; inset). The range of preferred spatial frequencies was higher for UVF neurons. Saturated colors show the mean/SEM of the individual curves. Also see Figure S5.

(C) Contrast sensitivity curves for three eccentricity-matched pairs of UVF/LVF neurons. Vertical lines indicate semi-saturation contrasts. UVF neurons had higher sensitivity.

(D) Summary of all contrast sensitivity curves. UVF neurons had lower semi-saturation contrasts and larger dynamic ranges.

Error bars indicate the SEM.

We also hypothesized that for memory-guided saccades (Experimental Procedures), RTs should not be affected by UVF/LVF location, because of stimulus absence and the deliberate task nature. However, UVF landing error should still decrease because of smaller motor RFs. We confirmed this (Figures S6C and S6D). Thus, our neural results have direct consequences for visual-motor behavior.

Anatomical Over-Representation of the Upper Visual Field

Finally, if UVF RFs are smaller than LVF RFs, then ensuring coverage of the UVF in a topographic map should recruit more neural tissue, analogous to foveal magnification. This suggests that the UVF should be over-represented. We found evidence for this by analyzing eccentricities and directions preferred by multi-unit visual activity first encountered at the SC surface (Experimental Procedures). We were noticeably more likely to encounter UVF than LVF locations. For example, Figure 6A shows a continuous run of daily recordings from one monkey, in which we systematically moved our recording electrode (laterally within a chamber) by 100-μm steps (or small multiples thereof). The figure shows electrode track locations along with directions and eccentricities encoded by multi-unit activity at the SC surface. A larger area of sites was dedicated to the UVF (Figure 6A, right panel), at least within the SC region that we could map given our display-system limits. Meta-analysis

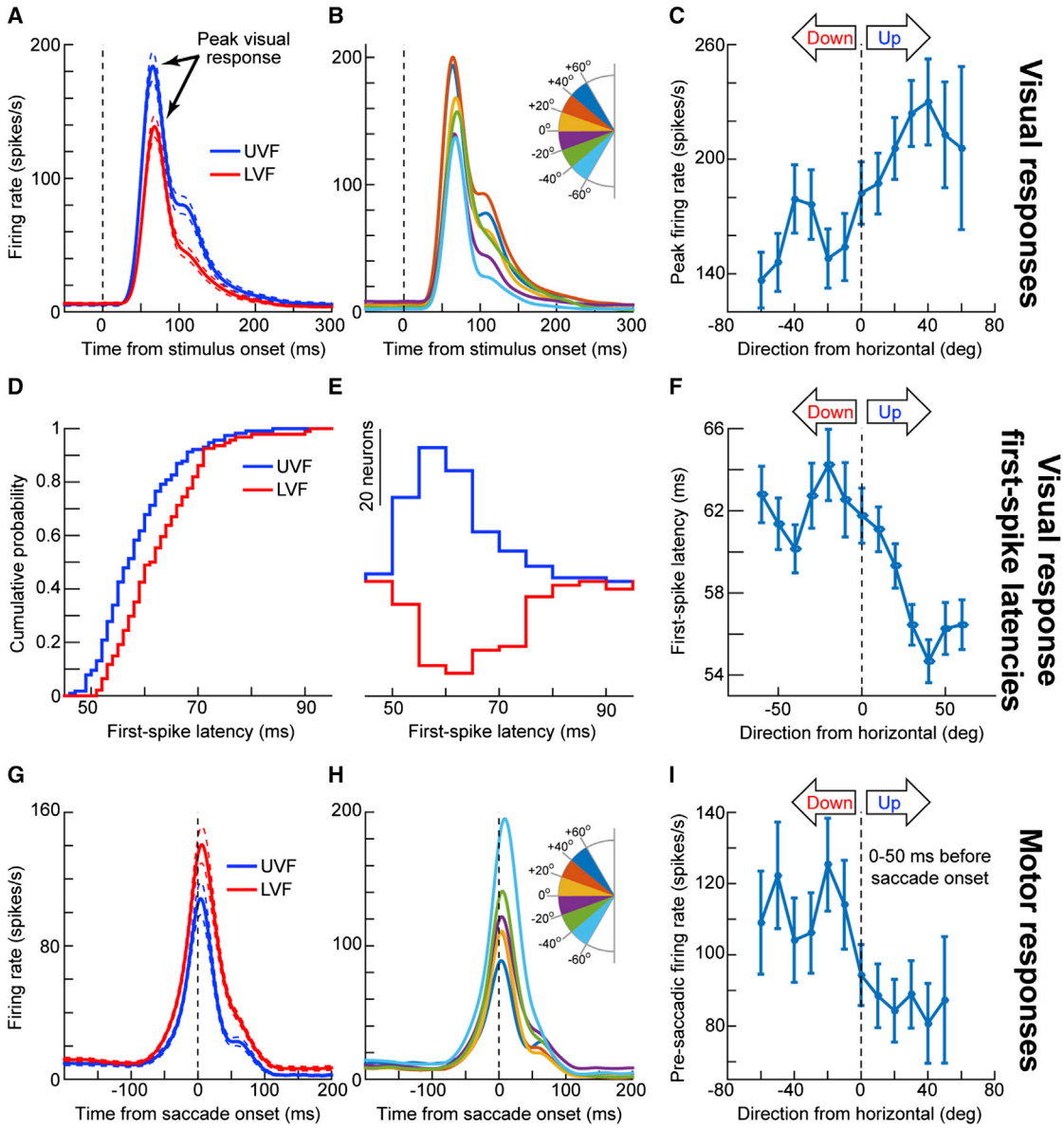

Figure 4. Stronger, Lower-Latency UVF Visual Responses

(A) Stimulus-evoked firing rate for UVF (blue) or LVF (red) neurons. In each neuron, the stimulus was a briefly flashed spot at the preferred RF hotspot. Peak firing rate was stronger in the UVF.

(B) Same data, but neurons were separated according to RF direction from horizontal (indicated by the color-coded legend). UVF responses were systematically higher.

(C) Same data, now summarized as a plot of peak stimulus-evoked firing rate versus RF direction from horizontal (similar binning to Figure 2B).

(D) Cumulative histograms of UVF or LVF first-spike latency (as computed in Figure 1D, and from the same task).

(E) Raw histograms of the data in (D). UVF responses occurred systematically sooner than LVF responses.

(F) Summary of first-spike latency as a function of RF direction from horizontal, as in (C).

(G–I) Same analyses as in (A)–(C), but for saccade-aligned firing rates during the delayed visually guided saccade task. Saccade-related activity showed the opposite patterns from visual activity (A–C).

Error bars indicate the SEM. Also see Figures 5, S4, and S6.

of electrode locations from an earlier study [13] revealed very similar results (Figure 6B). Thus, our observations are robust, even though they are very different from the universally accepted model of SC mapping [19], having identical UVF/LVF representations (Figure 6C). We therefore revised (Experimental Procedures) the model (Figure 6D) by including a functional discontinuity across the horizontal meridian.

An interesting consequence of our revised model is that it allows "equalizing" the size of the active SC population in anatomical coordinates, despite large changes in RF area as a function

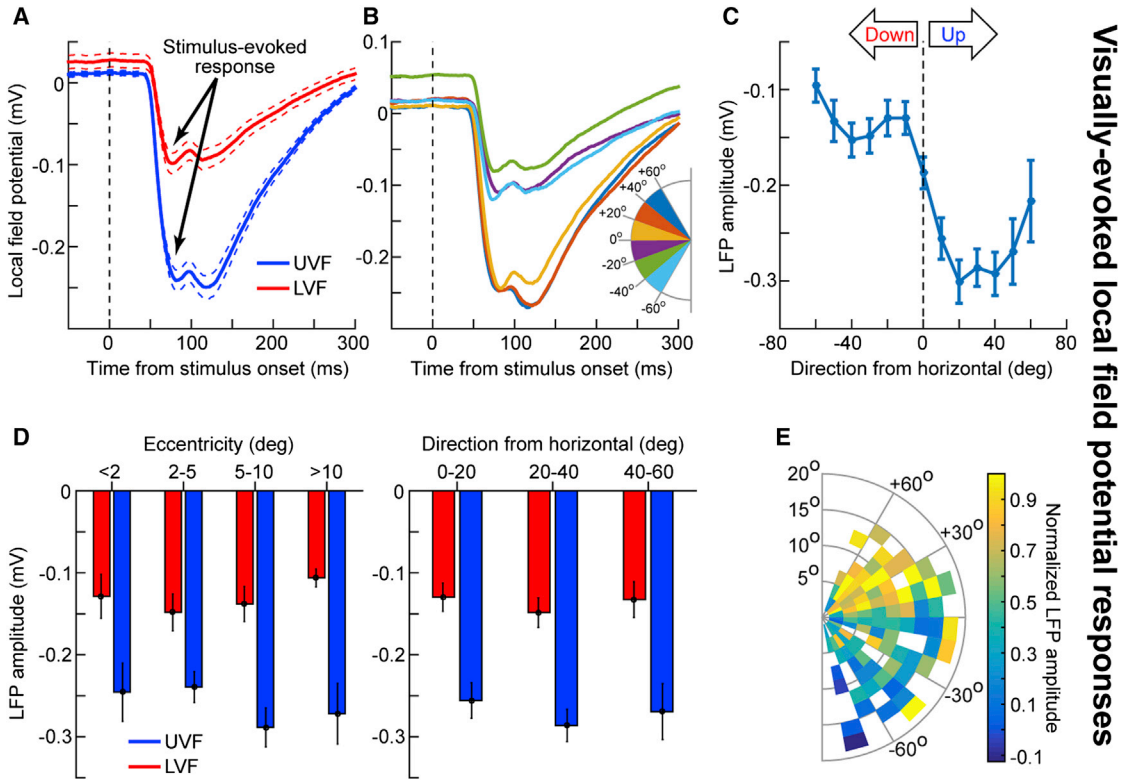

Figure 5. Stronger UVF Visually Evoked LFP Modulations

(A–C) Same analyses as in Figures 4A–4C, but for LFPs (Experimental Procedures). Peak LFP amplitude deflection (a negative-going deflection) was stronger in the UVF.

(D) We also separated electrode tracks according to their visual RF hotspot eccentricity and direction (x axis in each panel). Stronger negative deflections occurred in the UVF, regardless of eccentricity or direction. The LFP effect was much stronger than the firing rate effect (Figures 4A–4C).

(E) LFP visually evoked amplitude as a function of two-dimensional electrode location in the SC map (Experimental Procedures). The LFP response was stronger above the horizontal meridian.

Error bars indicate the SEM.

of either eccentricity or UVF/LVF location (e.g., Figure 2A). Specifically, in visual coordinates, UVF RFs are smaller than LVF RFs (Figures 7A and 7D), but our model suggests that there may be UVF magnification in SC coordinates, which compensates for this. We confirmed this in Figure 7. We projected visual RFs from retinotopic coordinates (Figures 7A and 7D) into SC anatomical coordinates using either the Ottes et al. model [19] (Figures 7B and 7E) or our revised model (Figures 7C and 7F). According to the original model, eccentricity is warped using logarithmic mapping. Thus, for either the UVF or LVF individually, RF sizes across eccentricities are equalized [9, 19] (compare eccentricities in each row individually in Figure 7B). However, because the original model is symmetric across the horizontal meridian, UVF RFs (upper row) are still smaller than the LVF RFs (bottom row). With our revised model (Figure 7C), over-representation of the UVF means that smaller UVF RFs in visual coordinates become "magnified" in SC coordinates. Thus, the SC can still equalize RF area both in terms of eccentricity (compare neurons in either the UVF or LVF individually in Figure 7C) and in terms of UVF or LVF location (compare neurons within a given column). Thus, even with UVF/LVF asymmetries, it may still be true that the same SC population size would be activated for different stimulus locations or saccade endpoints (Figure 7F), as was hypothesized earlier using horizontal saccades [9, 19]. Moreover, because motor RFs show similar effects to visual RFs (Figure 2), this also applies for the SC's motor map (Figure S7).

DISCUSSION

We observed a sharper, stronger, and lower-latency UVF representation in the primate SC, and also explored the behavioral and neuroanatomical consequences of these observations. Our results, showing an over-representation of the UVF (Figure 6), highlight the importance of analyzing structure-function relationships in the visual system.

Our results also motivate revisiting classic controversies about SC saccade-related dynamics. Specifically, peri-saccadic spreading of SC activity was hypothesized [9], but these results were hard to interpret and/or replicate [25]. These difficulties may have arisen exactly because of visual field locations. For example, much work on this issue used only horizontal saccades [9] or has used analyses assuming UVF/LVF symmetry [25]. However, if there are different UVF and LVF spatial pooling patterns (Figures 2, S3, and S4) and dynamics (Figures 4 and 5), then different "spreading" patterns (a hallmark of spatial pooling and lateral interaction [26]) may be expected to occur for UVF

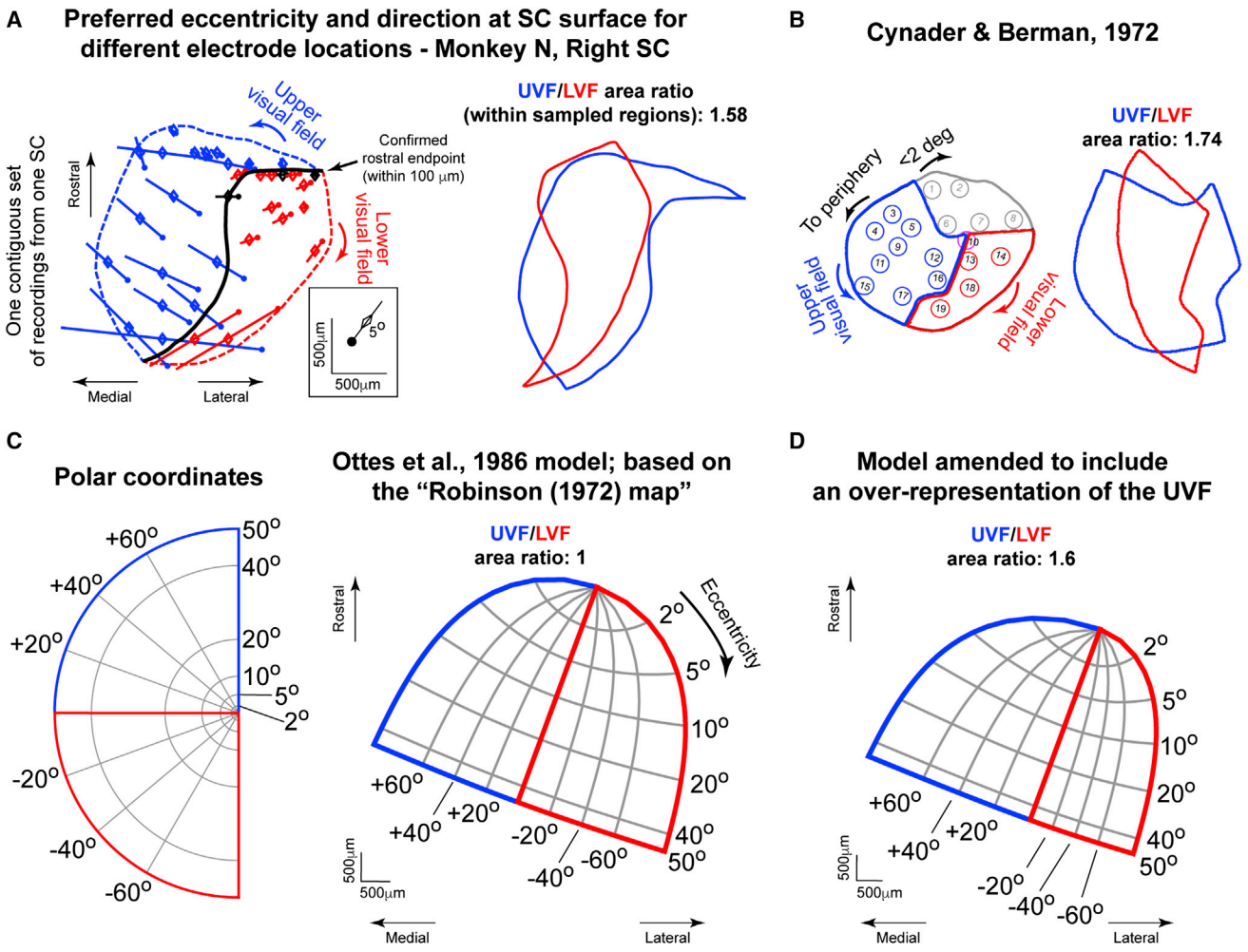

Figure 6. Over-Representation of the UVF in the Primate SC

(A) The left panel shows eccentricity and direction at the SC surface from one contiguous set of electrode penetrations. We mapped the rostral (foveal) SC with 100-μm resolution and a significant chunk of the caudal (peripheral) region. Each diamond indicates an electrode location; each colored line indicates eccentricity (length of line) and direction (direction of line, starting from the filled circle) encoded at the SC surface. Eccentricity is scaled according to the 5-degree diagonal line in the inset. Colors delineate UVF and LVF. The UVF representation was larger: the right panel summarizes the area within contours delineating UVF and LVF electrode tracks. Note that due to foveal magnification, neighboring locations in the rostral sites of the left panel appear to have similar directions and eccentricities to each other. However, we confirmed that preferred direction still consistently changes as a function of medio-lateral SC location across eccentricities (data not shown). In fact, in the most caudal sites of the left panel, where there is less foveal magnification, clearer medio-lateral changes in preferred directions can be seen [14].

(B) Meta-analysis of Cynader and Berman [13]. Shown are electrode locations, which we color coded according to the UVF and LVF (left). Because foveal neurons (gray color) were not described in [13], we excluded them from the meta-analysis. The UVF region is larger, and the area ratio of blue and red contours (right) is consistent with (A). Modified with permission from [13].

(C) A popular model of SC mapping, from Ottes et al. [19] and based on Robinson [14], having identical UVF/LVF representations.

(D) Our proposed revised model (Experimental Procedures).

Also see Figures 7 and S7.

versus LVF saccades. In fact, even though we did not explicitly sample deep "buildup" neurons showing the most convincing spreading [9], we nonetheless identified differences in UVF/LVF saccade-related spreading (Figure S4B). This result is further supported by a theoretical hypothesis on the effect of asymmetries in internal SC connections on population dynamics [26]. Thus, the UVF/LVF asymmetry that we uncovered can have a substantial impact on our understanding of saccade control by the SC.

Our results may also help identify functional sources of residual visual capabilities after brain lesions. For example, subjects without primary visual cortex lose conscious perception but still exhibit "blindsight" [42]. Blindsight, a residual visual capability, could primarily arise through a retino-tectal pathway [43] traversing the SC or an extra-striate retino-geniculate pathway through LGN [44]. Given that the SC UVF asymmetry may be the exact opposite [24] (see below) of potential asymmetries that are present in at least some cortical visual areas, like MT

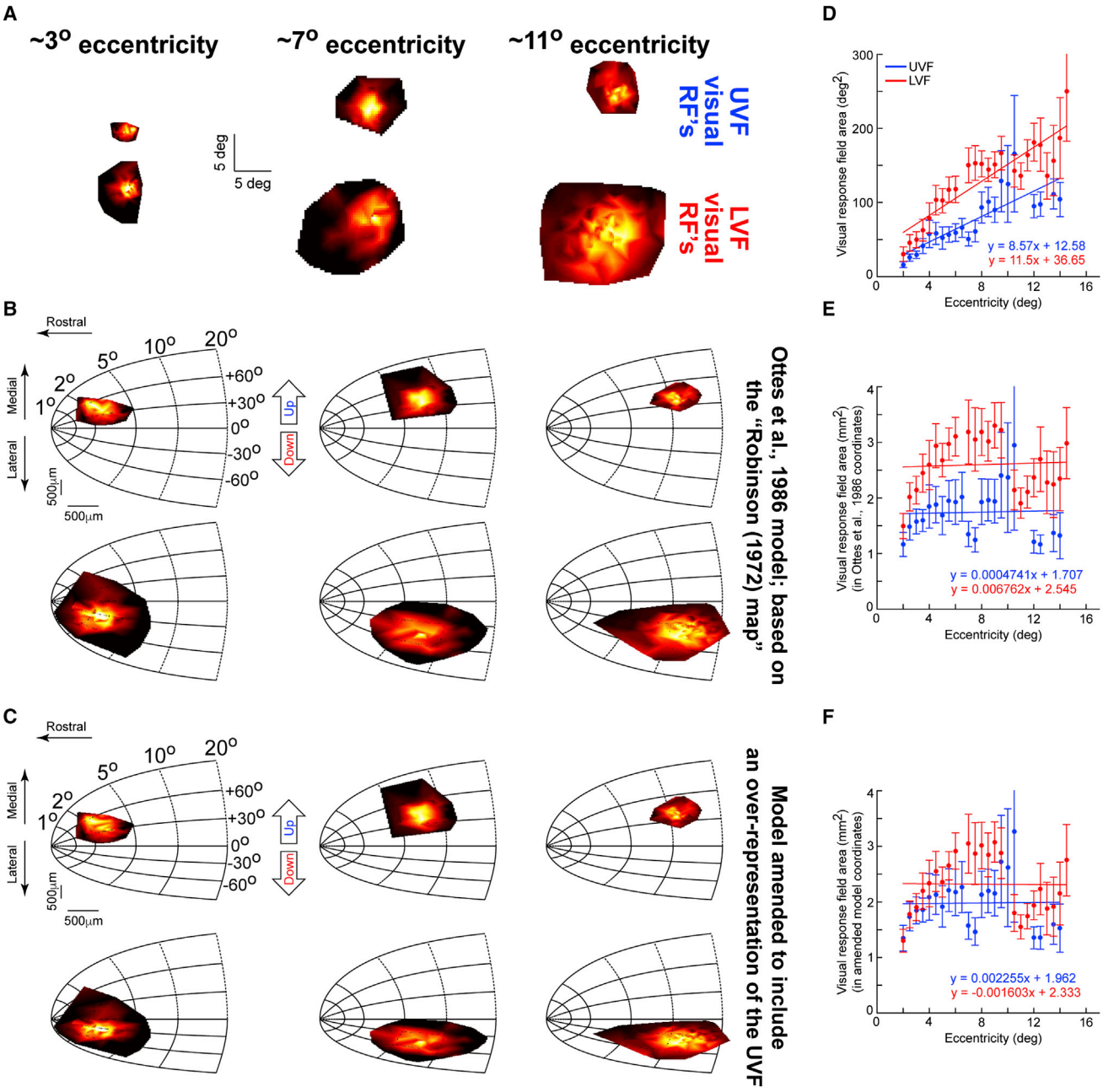

Figure 7. Implications of UVF Over-Representation on the Active SC Population Size for a Given Stimulus Location

(A) Example visual RFs from three eccentricity-matched pairs of UVF (top row) or LVF (bottom row) neurons. RF area increased with eccentricity and was larger in the LVF (Figure 2).

(B) The same RFs projected onto anatomical SC tissue using the Ottes et al. model [19] of the Robinson SC topographic map [9, 14, 19]. In each row (i.e., for either UVF or LVF neurons individually), RF sizes across the three eccentricities were roughly equalized (the most eccentric RF was decreased in size and the most central RF was magnified due to logarithmic warping). This is consistent with observations [9] made for horizontal saccades, and suggests that the size of the active SC population for a given saccade may be equalized in tissue coordinates [9, 19]. However, when different directions are considered, RFs cannot be equalized (compare the two rows).

(C) With our revised model (Figure 6D), the UVF is magnified. Thus, RF area can be equalized both in terms of eccentricity (compare neurons in either the UVF or LVF individually) and UVF/LVF location (compare neurons in a given eccentricity across the UVF or LVF).

(D) Population analysis similar to [9], showing dependence of RF area (in visual coordinates) on eccentricity and UVF/LVF location.

(E) The same data as in (D) plotted in SC coordinates using the original Ottes et al. model [19]. RF area was roughly equalized [9] in either the UVF or LVF (horizontal regression lines), but there was still a UVF/LVF asymmetry (the two regression lines are apart).

(F) The same data as in (D) and (E) plotted in revised SC coordinates. RF area was now roughly equalized not just for eccentricity but also for UVF/LVF location. Note that if the UVF magnification factor of the revised model is optimized further, the UVF/LVF differences that remain in this panel can be further reduced. Error bars indicate the SEM. Also see Figure S7.

[45], it could be the case that patterns of UVF versus LVF visual abilities/deficits exhibited in blindsight may help clarify on which alternative pathways blindsight subjects rely. For example, inspecting published saccade data from blindsight monkeys [46], we found that their patterns of landing errors were strongly consistent with what our results predict if the SC were a primary determinant of their performance. Thus, our results could resolve historical debates about the functional importance of the SC's visual analysis properties, some of which, like spatial-frequency tuning, are yet to be fully investigated.

Related to the above, it is not yet entirely clear which (or whether) early visual cortical areas would exhibit strong UVF/LVF asymmetries. It is sometimes assumed that V1 is symmetric [47], although there is variability among studies. It was also shown that MT over-represents the LVF [45]. However, because of an experimental bias to record from dorsal cortical tissue, and because work investigating detailed cortical topographies is quite old [45], much still remains to be learned about detailed UVF/LVF asymmetries in different visual and motor areas. Given Previc's hypotheses about ecological constraints on functional specialization in the visual system [24], one might make predictions. Specifically, Previc has hypothesized that areas analyzing properties of retinal images that typically occupy near space (e.g., having motion and stereo disparity patterns associated with near objects) might over-represent the LVF, and that areas needed for exploration of far space might over-represent the UVF [24]. Given this, the frontal eye field (FEF), implicated in eye-movement exploration, might exhibit UVF over-representation like the SC. Interestingly, in a recent study characterizing FEF RFs [48], ~70% of neurons were UVF neurons (51/73 in Figure 2D of [48]). Likewise, saccade-direction cells in entorhinal cortex exhibit a strong bias toward upward saccades [49]. Thus, UVF over-representation may emerge in a variety of areas implicated in visual exploration.

More generally, our results demonstrate that even for simple two-dimensional image maps, there exists remarkable optimization that goes well beyond foveal magnification. This idea is in line with emerging evidence that the visual system is well adapted to its environment. For example, mouse retinal photoreceptor distributions and spectral responses provide near-optimal sampling of the environment above and below the horizon [50]. Similarly, some mouse retinal ganglion cells have non-uniform topographies allowing them to preferentially enhance sampling of, say, frontal visual fields [51]. Finally, the mouse SC itself over-represents the UVF [52]. Thus, detailed specialization patterns within individual brain regions may be more pervasive than previously thought.

Finally, our results run contrary to a universally accepted model of SC topography [14, 19], which is used heavily to document, analyze, and interpret results. However, such interpretation might be misguided by pure symmetry assumptions. Our revised model (Figures 6D and 7) provides what we hope is a more useful tool for future studies of this important brain structure.

EXPERIMENTAL PROCEDURES

Animal Preparation

Ethics committees at the Tuebingen regional governmental offices approved the experiments. Monkeys P and N (male, *Macaca mulatta*, aged 7 years) were prepared earlier [32, 53, 54].

Behavioral Tasks

Visually Guided Saccade Task

A spot [32, 53, 54] was presented for 300–3,600 ms (monkey N) or 420–3,150 ms (monkey P). A white saccade target (1-degree-diameter circle) then appeared (5-degree eccentricity) in one of eight directions, and fixation was released. This task was used for behavioral tests (Figures S6A and S6B). We analyzed 24,396 (monkey N) and 17,446 (monkey P) trials.

Delayed Visually Guided Saccade Task

A spot was presented for 300–1,000 ms. An eccentric spot was then presented. The fixation spot was removed 500–1,000 ms later. Monkeys oriented to the eccentric spot. We collected >100 trials per neuron and varied target location to map visual and saccade-related RFs.

Memory-Guided Saccade Task

A spot was presented for 300–1,000 ms. An eccentric spot was flashed for ~50 ms. The fixation spot remained on for 300–1,100 ms before disappearing. Monkeys oriented toward the remembered flash location (within <2.5 degrees). We collected >45 trials per neuron, and placed the flash at the RF hotspot (assessed from the delayed visually guided saccade task or the fixation visual RF mapping task).

We used this task for classifying neurons as visual, visual-motor, or motor [32]. We also used it to study visual response strength and first-spike latency (Figures 1C, 1D, 4A–4F, and 5) because we had a well-controlled, repeatable stimulus location across trials (we also confirmed the observations with other tasks). Finally, we also analyzed additional saccade properties (see Figures S6C and S6D). We collected this task in 277 neurons.

Fixation Visual RF Mapping Task

In 78 neurons, we confirmed visual RF maps from the delayed visually guided saccade task by using a similar task involving fixation. The same sequence of events happened, except that the fixation spot was not removed at trial end. In a minority of neurons, we used this task instead of the saccade version for visual RF mapping. However, the two tasks were identical in the stimulus-induced phase.

Spatial-Frequency Tuning

Monkeys fixated a spot while we flashed a stationary vertical Gabor grating (80% contrast) filling the RF. Grating frequency was 0.56, 1.11, 2.22, 4.44, or 11.11 cycles/degree. Grating phase was randomized. We collected data from 106 neurons in this task.

Contrast Sensitivity

We analyzed data anew from [32], plus seven newly recorded neurons (total 110 neurons).

Data Analysis

When analyzing visual responses, we combined data from visual and visual-motor neurons because they showed similar results. Similarly, when analyzing motor responses, we combined motor and visual-motor neurons.

RF Areas

From the delayed visually guided saccade task or the fixation visual RF mapping task, we measured peak firing rate 30–150 ms after stimulus onset. We classified stimulus locations with activity >3 SDs from baseline (0–200 ms before stimulus onset) as being within the visual RF (e.g., dots in Figure 1B). We also Delaunay triangulated locations and linearly interpolated to generate three-dimensional surfaces (e.g., Figure 1B). We measured the area of all significant locations. The RF hotspot was the location with maximal activity. For motor RFs, we repeated the same procedure but measured mean presaccadic (within 50 ms) firing rate.

For Figures 2A and 2E, we binned eccentricities into 1.5-degree bins (with running windows of 0.5-degree step size and a minimum of seven neurons per bin). We could not map RF area at very large eccentricities because of display-system constraints. For a given eccentricity range (Figure 2B), we also binned RF directions into 20-degree bins (in steps of 10 degrees and a minimum of ten neurons per bin).

Spatial-Frequency Tuning

We only analyzed trials without microsaccades <100 ms from stimulus onset. We measured peak visual response 20–150 ms after grating onset. We constructed tuning curves according to

$$f.r.(sf) = a_1 e^{-\left(\frac{sf-b_1}{c_1}\right)^2} - a_2 e^{-\left(\frac{sf-b_2}{c_2}\right)^2} + B, \qquad \text{(Equation 1)}$$

where *f.r.* is firing rate, *sf* is spatial frequency, *B* is baseline firing rate, and a_1, b_1, c_1, a_2, b_2, and c_2 are parameters. The spatial frequency for which Equation 1 peaked was the preferred spatial frequency. To facilitate visualizing preferences across neurons (e.g., Figure 3B), we normalized curves by their maximum.

Contrast Sensitivity

We fit mean visual response 50–150 ms after grating onset using [32]

$$f.r.(c) = R\frac{c^n}{c_{50}^n + c^n} + B, \qquad \text{(Equation 2)}$$

where *c* is contrast. For dynamic range, we calculated the difference between maximum and minimum in a fitted curve. We also only analyzed no-microsaccade trials.

First-Spike Latency

We analyzed neurons with zero baseline activity (i.e., the majority). We manually defined time ranges after stimulus onset and searched for first spikes. Figure 4F binning was like in Figure 2B.

LFP analyses, population reconstruction, SC surface topography estimates, and modeling are described in detail in the Supplemental Experimental Procedures.

SUPPLEMENTAL INFORMATION

Supplemental Information includes Supplemental Experimental Procedures and seven figures and can be found with this article online at http://dx.doi.org/10.1016/j.cub.2016.04.059.

AUTHOR CONTRIBUTIONS

Z.M.H. and C.-Y.C. performed the experiments and analyzed the data. Z.M.H. wrote the paper.

ACKNOWLEDGMENTS

The authors were funded by the Werner Reichardt Centre for Integrative Neuroscience (CIN) at the Eberhard Karls University of Tuebingen. The CIN is an Excellence Cluster funded by the Deutsche Forschungsgemeinschaft (DFG) within the framework of the Excellence Initiative (EXC 307).

Received: February 12, 2016
Revised: March 23, 2016
Accepted: April 22, 2016
Published: June 9, 2016

REFERENCES

1. Wurtz, R.H., and Albano, J.E. (1980). Visual-motor function of the primate superior colliculus. Annu. Rev. Neurosci. *3*, 189–226.
2. Gandhi, N.J., and Katnani, H.A. (2011). Motor functions of the superior colliculus. Annu. Rev. Neurosci. *34*, 205–231.
3. Krauzlis, R.J., Lovejoy, L.P., and Zénon, A. (2013). Superior colliculus and visual spatial attention. Annu. Rev. Neurosci. *36*, 165–182.
4. Dash, S., Yan, X., Wang, H., and Crawford, J.D. (2015). Continuous updating of visuospatial memory in superior colliculus during slow eye movements. Curr. Biol. *25*, 267–274.
5. Klier, E.M., Wang, H., and Crawford, J.D. (2001). The superior colliculus encodes gaze commands in retinal coordinates. Nat. Neurosci. *4*, 627–632.
6. Goossens, H.H., and van Opstal, A.J. (2012). Optimal control of saccades by spatial-temporal activity patterns in the monkey superior colliculus. PLoS Comput. Biol. *8*, e1002508.
7. Goossens, H.H., and Van Opstal, A.J. (2006). Dynamic ensemble coding of saccades in the monkey superior colliculus. J. Neurophysiol. *95*, 2326–2341.
8. Munoz, D.P., and Wurtz, R.H. (1995). Saccade-related activity in monkey superior colliculus. I. Characteristics of burst and buildup cells. J. Neurophysiol. *73*, 2313–2333.
9. Munoz, D.P., and Wurtz, R.H. (1995). Saccade-related activity in monkey superior colliculus. II. Spread of activity during saccades. J. Neurophysiol. *73*, 2334–2348.
10. McPeek, R.M., and Keller, E.L. (2004). Deficits in saccade target selection after inactivation of superior colliculus. Nat. Neurosci. *7*, 757–763.
11. Carello, C.D., and Krauzlis, R.J. (2004). Manipulating intent: evidence for a causal role of the superior colliculus in target selection. Neuron *43*, 575–583.
12. Sadeh, M., Sajad, A., Wang, H., Yan, X., and Crawford, J.D. (2015). Spatial transformations between superior colliculus visual and motor response fields during head-unrestrained gaze shifts. Eur. J. Neurosci. *42*, 2934–2951.
13. Cynader, M., and Berman, N. (1972). Receptive-field organization of monkey superior colliculus. J. Neurophysiol. *35*, 187–201.
14. Robinson, D.A. (1972). Eye movements evoked by collicular stimulation in the alert monkey. Vision Res. *12*, 1795–1808.
15. Sparks, D.L., and Nelson, I.S. (1987). Sensory and motor maps in the mammalian superior colliculus. Trends Neurosci. *10*, 312–317.
16. Hinton, G.E., McClelland, J.L., and Rumelhart, D.E. (1986). Distributed representations. In Parallel Distributed Processing: Explorations in the Microstructure of Cognition, Volume 1: Foundations, D.E. Rumelhart, and J.L. McClelland, eds. (MIT Press), pp. 77–109.
17. Pouget, A., Dayan, P., and Zemel, R. (2000). Information processing with population codes. Nat. Rev. Neurosci. *1*, 125–132.
18. Lee, C., Rohrer, W.H., and Sparks, D.L. (1988). Population coding of saccadic eye movements by neurons in the superior colliculus. Nature *332*, 357–360.
19. Ottes, F.P., Van Gisbergen, J.A., and Eggermont, J.J. (1986). Visuomotor fields of the superior colliculus: a quantitative model. Vision Res. *26*, 857–873.
20. Ko, H.K., Poletti, M., and Rucci, M. (2010). Microsaccades precisely relocate gaze in a high visual acuity task. Nat. Neurosci. *13*, 1549–1553.
21. Tian, X., Yoshida, M., and Hafed, Z.M. (2016). A microsaccadic account of attentional capture and inhibition of return in Posner cueing. Front. Syst. Neurosci. *10*, 23.
22. Hafed, Z.M., Goffart, L., and Krauzlis, R.J. (2009). A neural mechanism for microsaccade generation in the primate superior colliculus. Science *323*, 940–943.
23. Hafed, Z.M., and Krauzlis, R.J. (2012). Similarity of superior colliculus involvement in microsaccade and saccade generation. J. Neurophysiol. *107*, 1904–1916.
24. Previc, F.H. (1990). Functional specialization in the lower and upper visual fields in humans: its ecological origins and neurophysiological implications. Behav. Brain Sci. *13*, 519–542.
25. Anderson, R.W., Keller, E.L., Gandhi, N.J., and Das, S. (1998). Two-dimensional saccade-related population activity in superior colliculus in monkey. J. Neurophysiol. *80*, 798–817.
26. Nakahara, H., Morita, K., Wurtz, R.H., and Optican, L.M. (2006). Saccade-related spread of activity across superior colliculus may arise from asymmetry of internal connections. J. Neurophysiol. *96*, 765–774.
27. Choi, W.Y., and Guitton, D. (2009). Firing patterns in superior colliculus of head-unrestrained monkey during normal and perturbed gaze saccades reveal short-latency feedback and a sluggish rostral shift in activity. J. Neurosci. *29*, 7166–7180.
28. Goldberg, M.E., and Wurtz, R.H. (1972). Activity of superior colliculus in behaving monkey. I. Visual receptive fields of single neurons. J. Neurophysiol. *35*, 542–559.
29. Rubin, N., Nakayama, K., and Shapley, R. (1996). Enhanced perception of illusory contours in the lower versus upper visual hemifields. Science *271*, 651–653.

30. De Valois, K.K., De Valois, R.L., and Yund, E.W. (1979). Responses of striate cortex cells to grating and checkerboard patterns. J. Physiol. *291*, 483–505.

31. De Valois, R.L., and De Valois, K.K. (1980). Spatial vision. Annu. Rev. Psychol. *31*, 309–341.

32. Chen, C.Y., Ignashchenkova, A., Thier, P., and Hafed, Z.M. (2015). Neuronal response gain enhancement prior to microsaccades. Curr. Biol. *25*, 2065–2074.

33. Boehnke, S.E., and Munoz, D.P. (2008). On the importance of the transient visual response in the superior colliculus. Curr. Opin. Neurobiol. *18*, 544–551.

34. Hafed, Z.M., Chen, C.-Y., and Tian, X. (2015). Vision, perception, and attention through the lens of microsaccades: mechanisms and implications. Front. Syst. Neurosci. *9*, 167.

35. Hafed, Z.M., and Krauzlis, R.J. (2010). Microsaccadic suppression of visual bursts in the primate superior colliculus. J. Neurosci. *30*, 9542–9547.

36. Schlykowa, L., Hoffmann, K.P., Bremmer, F., Thiele, A., and Ehrenstein, W.H. (1996). Monkey saccadic latency and pursuit velocity show a preference for upward directions of target motion. Neuroreport *7*, 409–412.

37. Zhou, W., and King, W.M. (2002). Attentional sensitivity and asymmetries of vertical saccade generation in monkey. Vision Res. *42*, 771–779.

38. Cerkevich, C.M., Lyon, D.C., Balaram, P., and Kaas, J.H. (2014). Distribution of cortical neurons projecting to the superior colliculus in macaque monkeys. Eye Brain *2014*, 121–137.

39. Van Essen, D.C. (1979). Visual areas of the mammalian cerebral cortex. Annu. Rev. Neurosci. *2*, 227–263.

40. Felleman, D.J., and Van Essen, D.C. (1991). Distributed hierarchical processing in the primate cerebral cortex. Cereb. Cortex *1*, 1–47.

41. Fischer, B., and Boch, R. (1983). Saccadic eye movements after extremely short reaction times in the monkey. Brain Res. *260*, 21–26.

42. Leopold, D.A. (2012). Primary visual cortex: awareness and blindsight. Annu. Rev. Neurosci. *35*, 91–109.

43. Kato, R., Takaura, K., Ikeda, T., Yoshida, M., and Isa, T. (2011). Contribution of the retino-tectal pathway to visually guided saccades after lesion of the primary visual cortex in monkeys. Eur. J. Neurosci. *33*, 1952–1960.

44. Schmid, M.C., Mrowka, S.W., Turchi, J., Saunders, R.C., Wilke, M., Peters, A.J., Ye, F.Q., and Leopold, D.A. (2010). Blindsight depends on the lateral geniculate nucleus. Nature *466*, 373–377.

45. Van Essen, D.C., Maunsell, J.H., and Bixby, J.L. (1981). The middle temporal visual area in the macaque: myeloarchitecture, connections, functional properties and topographic organization. J. Comp. Neurol. *199*, 293–326.

46. Yoshida, M., Takaura, K., Kato, R., Ikeda, T., and Isa, T. (2008). Striate cortical lesions affect deliberate decision and control of saccade: implication for blindsight. J. Neurosci. *28*, 10517–10530.

47. He, S., Cavanagh, P., and Intriligator, J. (1996). Attentional resolution and the locus of visual awareness. Nature *383*, 334–337.

48. Mayo, J.P., DiTomasso, A.R., Sommer, M.A., and Smith, M.A. (2015). Dynamics of visual receptive fields in the macaque frontal eye field. J. Neurophysiol. *114*, 3201–3210.

49. Killian, N.J., Potter, S.M., and Buffalo, E.A. (2015). Saccade direction encoding in the primate entorhinal cortex during visual exploration. Proc. Natl. Acad. Sci. USA *112*, 15743–15748.

50. Baden, T., Schubert, T., Chang, L., Wei, T., Zaichuk, M., Wissinger, B., and Euler, T. (2013). A tale of two retinal domains: near-optimal sampling of achromatic contrasts in natural scenes through asymmetric photoreceptor distribution. Neuron *80*, 1206–1217.

51. Bleckert, A., Schwartz, G.W., Turner, M.H., Rieke, F., and Wong, R.O. (2014). Visual space is represented by nonmatching topographies of distinct mouse retinal ganglion cell types. Curr. Biol. *24*, 310–315.

52. Dräger, U.C., and Hubel, D.H. (1976). Topography of visual and somatosensory projections to mouse superior colliculus. J. Neurophysiol. *39*, 91–101.

53. Chen, C.Y., and Hafed, Z.M. (2013). Postmicrosaccadic enhancement of slow eye movements. J. Neurosci. *33*, 5375–5386.

54. Hafed, Z.M., and Ignashchenkova, A. (2013). On the dissociation between microsaccade rate and direction after peripheral cues: microsaccadic inhibition revisited. J. Neurosci. *33*, 16220–16235.

Current Biology, Volume *26*

Supplemental Information

Sharper, Stronger, Faster Upper Visual Field Representation in Primate Superior Colliculus

Ziad M. Hafed and Chih-Yang Chen

Supplemental Figures

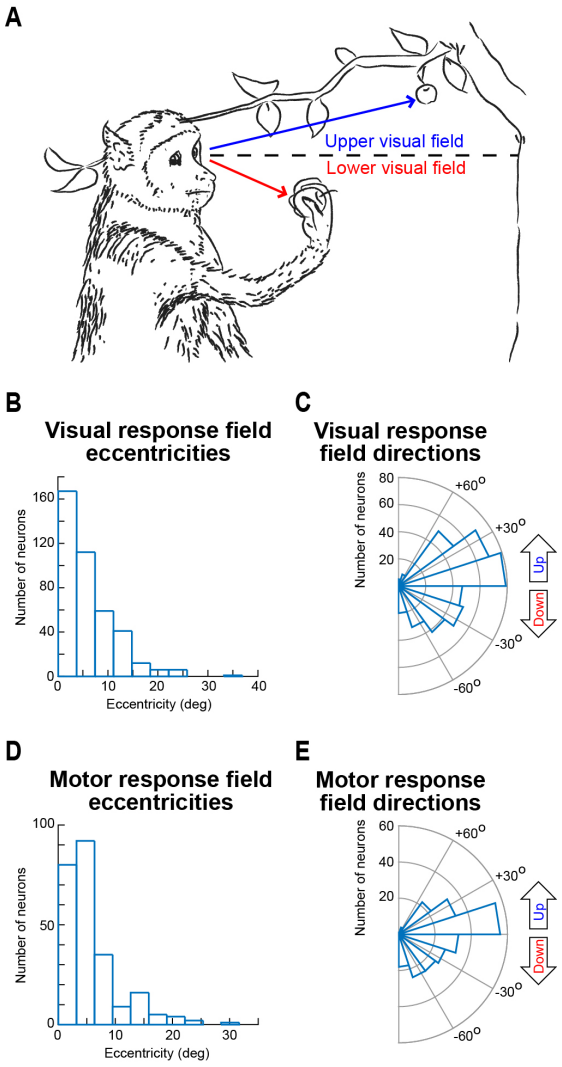

Figure S1, Related to Figure 1. (**A**) A situation similar to that shown in Fig. 1A, but using an example of a monkey in its natural habitat (modified with permission from [S1]). Relative to the line of sight (dashed black line), the apple in the LVF is closer to the monkey than the apple in the UVF. The LVF apple would thus project a larger retinal image. (**B-E**) Locations of SC visual and motor (saccade-related) RF's recorded for the current study. (**B, D**) RF hotspot eccentricities across neurons. (**C, E**) RF hotspot directions from horizontal. Note that we sampled neurons in both the right and left SC in both monkeys. However, in (**C, E**), we show directions collapsed together into one side of space, in order to facilitate presentation of the range of UVF/LVF directions that we sampled. Fig. S2 shows controls when only the right or left SC was analyzed. Also, note that we collected samples in many directions (from predominantly pure down to predominantly pure up). However, we had relatively fewer samples beyond +/- 60 deg from horizontal. Thus, even though we still showed individual examples from beyond +/- 60 deg (e.g. Fig. S2C), our summary plots were primarily restricted to the directions with maximal support in our population (and similarly for eccentricity summaries).

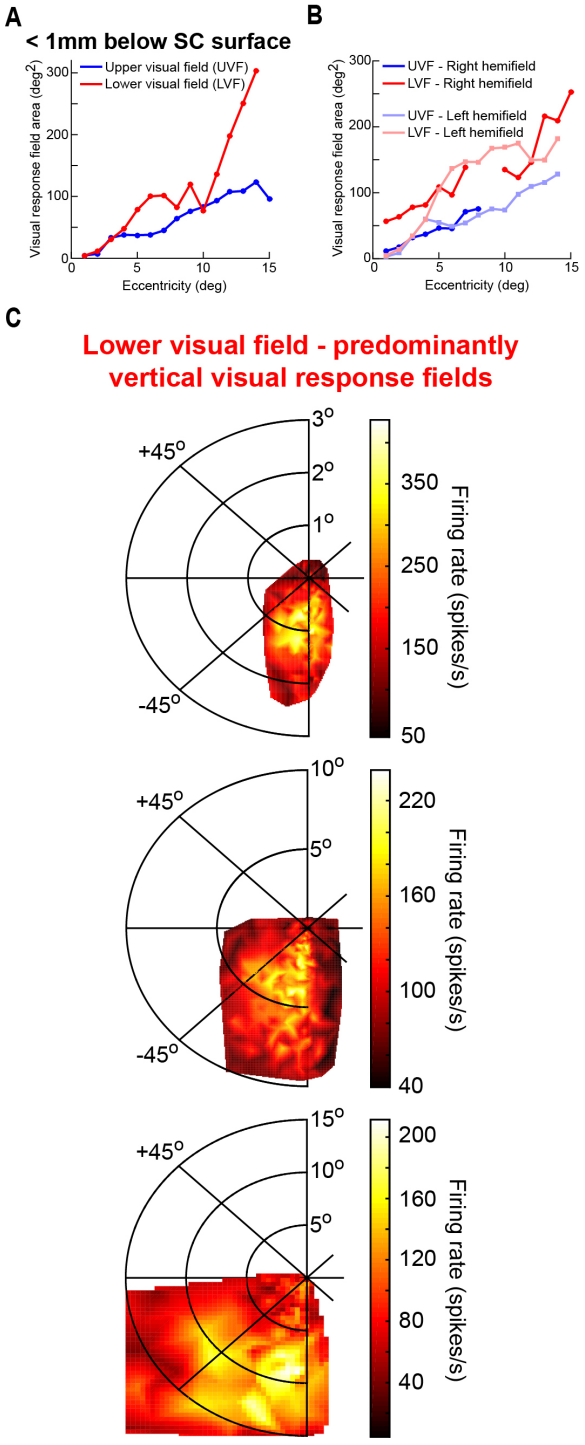

Figure S2, Related to Figure 2. (**A, B**) Analyses similar to those in Fig. 2A, but restricted to only superficial SC layers (**A**) or one side of space (**B**). (**A**) indicates that even the most superficial layer neurons show an UVF/LVF asymmetry in RF area. A 2-way ANOVA revealed statistically significant main effects of both eccentricity and UVF/LVF location ($p<0.05$ for each main factor). Similar analyses for deeper neurons (>1 mm) also revealed significant main effects of eccentricity and UVF/LVF location. Thus, the effect in Fig. 2A is not an artifact of sampling deeper neurons with larger RF's. Also, note that our behavioral effects (Fig. S6), as well as motor RF area effects (Figs. 2D,E, S3), support the conclusion that

the asymmetry seen in Fig. 2A is a functional property of SC architecture and not an analysis artifact. The sample neurons presented in Fig. 1 (having similar depth and RF hotspot eccentricity) also support this conclusion. (**B**) indicates that a similar UVF/LVF asymmetry in RF area existed in either the left or right SC, representing either the right or left visual hemifield, respectively. We confirmed this statistically: for either the right or left hemifield individually, a 2-way ANOVA confirmed that RF area depended on both main factors of eccentricity and UVF/LVF location ($p<0.05$ for each main effect). (**C**) Example visual RF's for predominantly vertical neurons in the LVF. We noticed elongated RF shapes for such neurons, and the RF's had a relatively large extent even for the top-most central neuron (notice the eccentricity scale bar for each neuron). In our experiments, predominantly vertical UVF neurons did not seem to exhibit such elongation and size increase, at least not in our recorded sample of neurons.

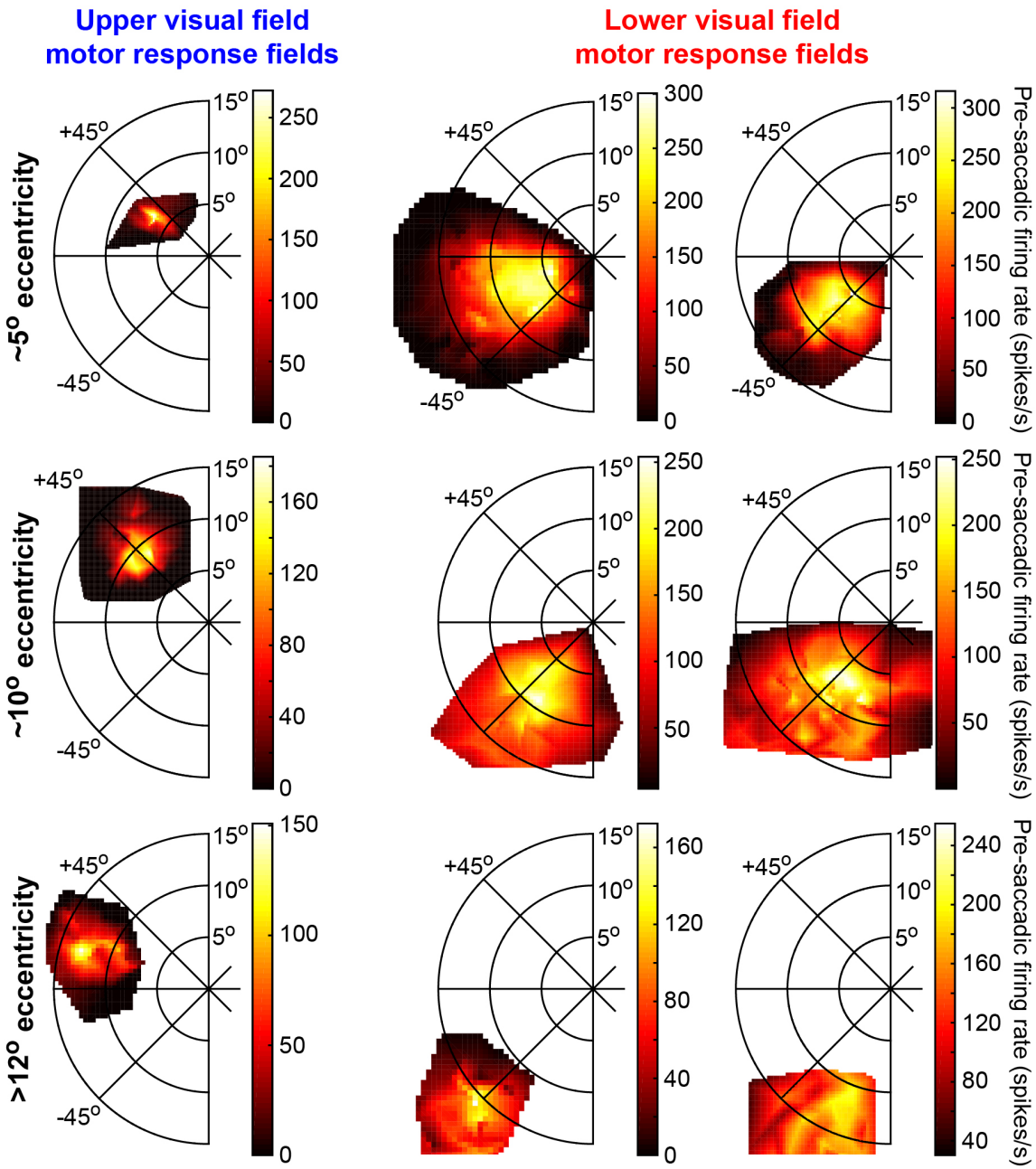

Figure S3, Related to Figure 2. Example saccade-related motor RF's for UVF and LVF SC neurons. Each row shows 3 example neurons from a given RF hotspot eccentricity. In each row, the leftmost neuron is an UVF neuron, and the rightmost two neurons are LVF neurons closely matched in eccentricity. As can be seen, the UVF neurons had motor RF's that were consistently smaller than the motor RF's of LVF neurons. Thus, higher-resolution UVF spatial representation in the primate SC extends to the efferent saccade-related maps of this structure (also see Fig. 2E). This is consistent with behavioral properties of saccades, even in the absence of a visual stimulus (Fig. S6). Note that in the top row, the leftmost two example neurons shown here are the same as those shown in Fig. 2D. They are included here to facilitate comparison to the rightmost neuron having a closely matched motor RF hotspot eccentricity.

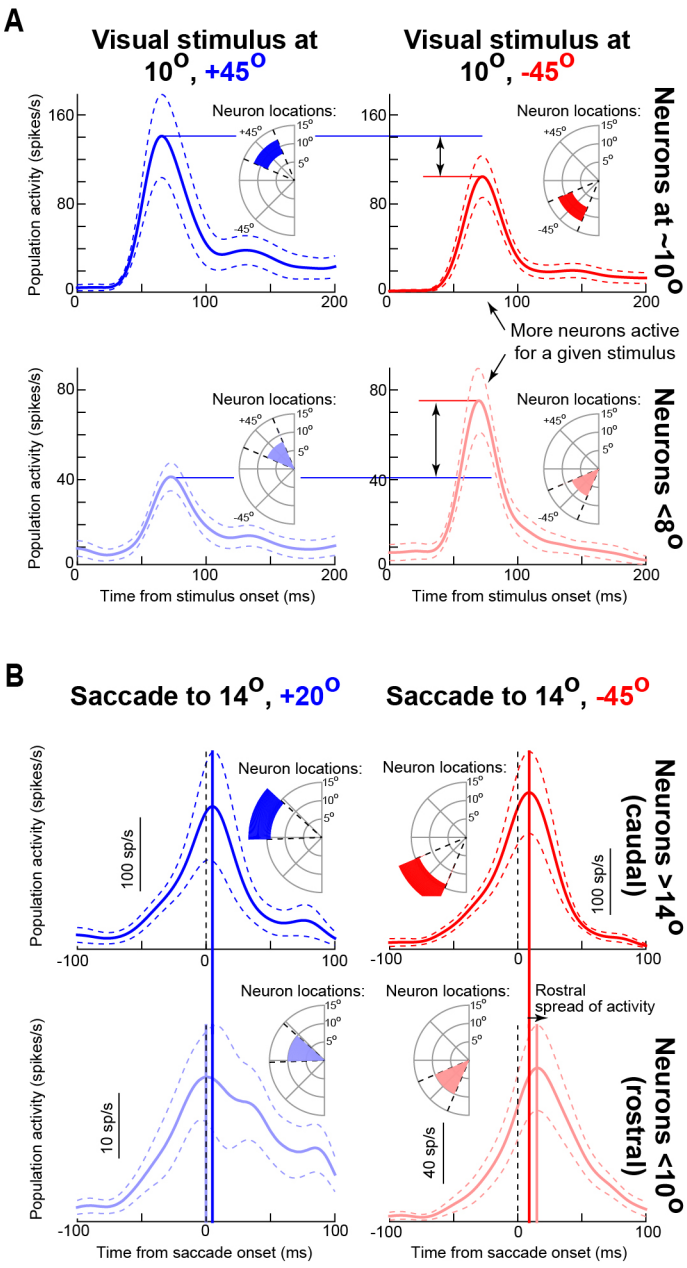

Figure S4, Related to Figures 2, 4, 5. Population reconstruction of SC activity following the presentation of a visual stimulus at a single location (**A**) or during the generation of a saccade to a specific endpoint (**B**). (**A**) In the left column, we asked how different SC neurons would be activated for a stimulus presented at 10 deg eccentricity and +45 deg above the horizontal meridian (from the delayed visually-guided saccade task, Experimental Procedures). For all presentations of this stimulus, we measured the activity of all neurons regardless of their visual RF hotspot location. We then plotted the responses of neurons with RF hotspots either close to the stimulus location (upper row, saturated blue) or of neurons with more central RF hotspot locations (bottom row, faint blue). We repeated the same analysis in the right column, but for a stimulus (and neurons) in the LVF. As can be seen, in the UVF, the more central neurons were much less active than the neurons with hotspot location near the stimulus location (compare the bottom and top panels in the left column). This is expected since more central neurons prefer more central locations than 10 deg, and UVF RF's are small (Figs. 1-2). However, for the LVF condition (right column), the change in firing rate between the top and bottom panels is smaller. This indicates that, because of their larger RF's, neurons whose RF hotspot locations are farther away from the stimulus would be more likely to still "see" the

stimulus in the LVF than in the UVF. Thus, our results of UVF/LVF differences in visual RF area have implications on population coding schemes in the SC (also see Figs. 7, S7). Also note that neurons at the preferred stimulus location were more active in the UVF than in the LVF (compare the top two panels), consistent with Figs. 1, 4A-C, 5. (**B**) Potential implication of saccade-related firing rate and RF area asymmetries on historically contentious debates about the SC's role in saccade generation. We performed a similar reconstruction of population activity to that performed in (**A**). However, this time, we reconstructed saccade-related activity (instead of visually-evoked activity) for two example saccades (from the delayed visually-guided saccade task, Experimental Procedures): one to the UVF (left column) and one to the LVF (right column). The solid vertical lines show the times of peak saccade-related discharge in each panel. Besides the fact that the more central neurons (compare the bottom two panels, noting the difference in scale bars) were more active in the LVF condition than in the UVF condition (confirming **A**), we also found an additional asymmetry in the motor responses. Specifically, in the LVF condition (right column), more central neurons show a later peak discharge than more peripheral neurons encoding the actual saccade endpoint (compare vertical saturated and faint red lines). This effect means that central neurons become activated later than peripheral neurons (akin to a spread of activity during the saccade) [S2]. This effect was absent for a similarly sized saccade in the UVF (left column). We also replicated the effect for other large saccade amplitudes (>10 deg). We should emphasize here that we did not explicitly sample "buildup" SC neurons, for which the spread has been most robustly reported in the literature [S2]. Nonetheless, we still see evidence of an effect even in our more superficial visual-motor neurons, and, more importantly, we also see evidence that this phenomenon might critically depend on UVF/LVF asymmetries. This makes sense in retrospect, because such spreading of activity is expected to depend on lateral interactions [S3], which our results suggest might be very different in the UVF and LVF. Also, note that the effect in the right column is small, which is consistent with evidence that saccade-related spreading occurs most robustly for saccades >20-30 deg [S4], which are larger than those we investigated here. Error bars in all panels denote s.e.m.

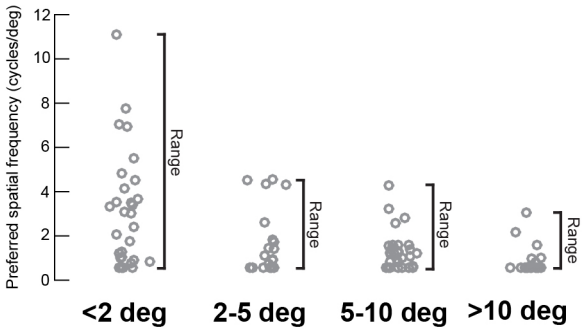

Figure S5, Related to Figure 3. Preferred spatial frequencies of individual SC neurons at different retinotopic eccentricities. Each circle represents a neuron (note that we jittered the horizontal position of the circles within a column in order to avoid multiple neurons from masking each other). Consistent with cortical visual areas, neurons at a given eccentricity exhibited a range of preferred spatial frequencies (square brackets highlight the ranges of spatial-frequency channels observed in each eccentricity range). Thus, multiple spatial-frequency channels are represented within a given eccentricity in the SC. Moreover, and again consistent with cortical visual areas, spatial-frequency preferences consistently decreased with increasing retinotopic eccentricity ($p<0.05$, 1-way ANOVA with eccentricity as the main factor). Thus, the SC becomes increasingly low-pass in the periphery. The main text shows that in addition to the properties shown in this figure, there are also UVF/LVF asymmetries in spatial-frequency channels in the SC (Fig. 3A, B).

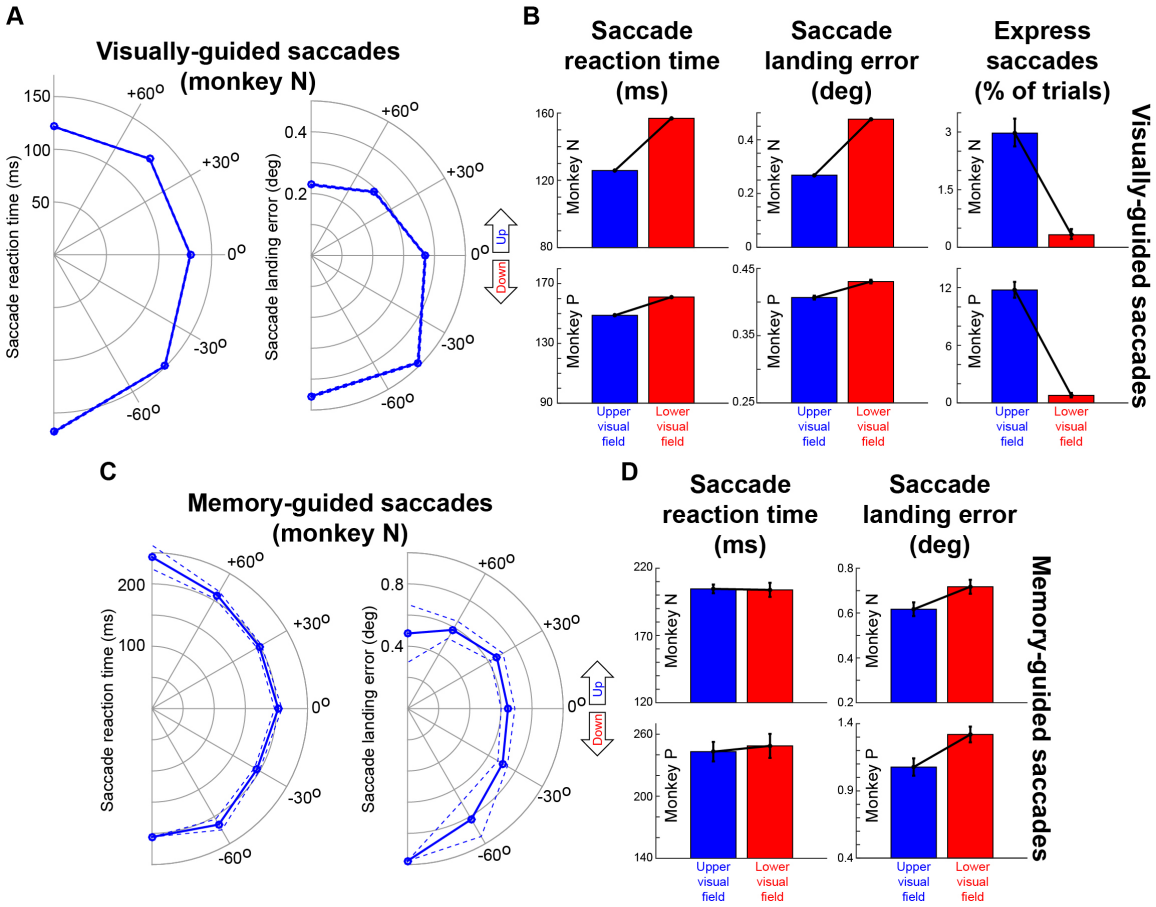

Figure S6, Related to Figures 2, 4, 5. Lower-latency, more accurate UVF saccades. (**A**) Saccadic RT (left) and landing error (right) as a function of target location during immediate, visually-guided saccades from one monkey. Right/left target locations were collapsed onto one side to facilitate viewing of UVF/LVF effects. Both RT and landing error decreased in the UVF ($p<0.05$, two-tailed t-test between UVF and LVF locations for each of RT and landing error). The RT effect likely reflects stronger and lower-latency UVF SC visual bursts, and the landing error effect likely reflects smaller UVF visual and motor RF areas. (**B**) The leftmost two columns summarize the results in (**A**) for each of the two monkeys. In both monkeys, RT and landing error were smaller in the UVF ($p<0.05$, two-tailed t-test). In the rightmost column, we plotted the likelihood of express saccades in the same data. There was a 9-fold to 14-fold increase in express saccade probability in the UVF (error bars in this column show 95% confidence intervals and demonstrate the statistical significance of the result). This is a strong effect given that express saccades are expected to be rare or completely absent in this kind of immediate, visually-guided saccade task. (**C**) For memory-guided saccades, RT's were not affected by visual field location (left panel; $p>0.05$, two-tailed t-test between UVF and LVF locations), but landing error decreased in the UVF (right panel; $p<0.05$, two-tailed t-test). The lack of RT effect is expected because of the prior knowledge about target location provided in this memory-guided saccade task (Experimental Procedures), but there was still a landing error effect likely reflecting smaller UVF motor RF areas. (**D**) This effect was consistent across the two monkeys: RT was not shorter in the UVF ($p>0.05$, two-tailed t-test) but landing error was still smaller ($p<0.05$, two-tailed t-test). Note that for memory-guided saccade data, we restricted analyses to eye movements <8 deg in amplitude, to be in line with (**A, B**). Error bars, when visible, denote s.e.m., except for express saccade proportions (in which case they denote 95% confidence intervals as stated above).

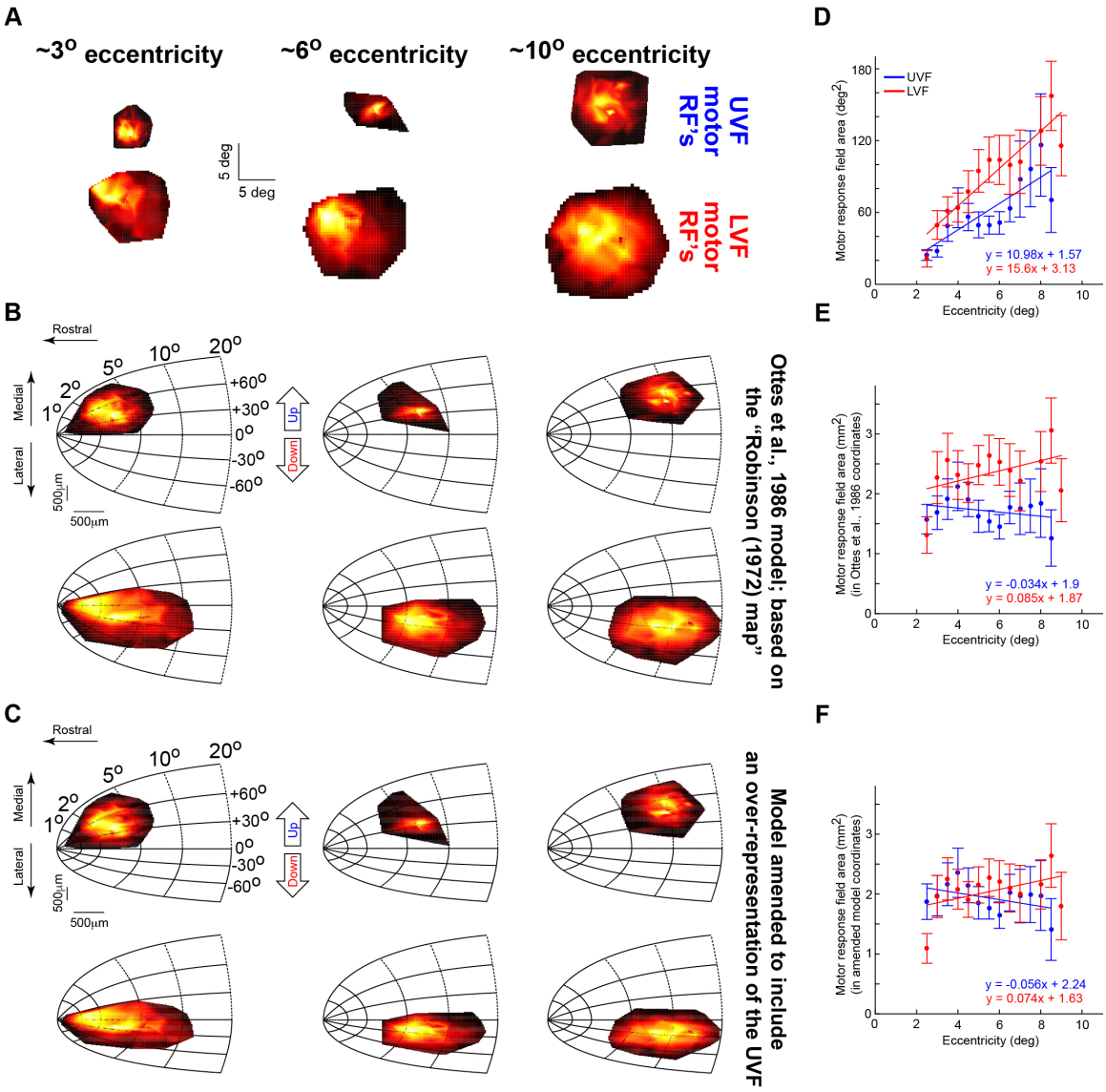

Figure S7, Related to Figure 7. Implications of an over-representation of the UVF on the size of the active SC population for a given saccade endpoint. This figure is identical in format to that in Fig. 7. However, in the current analysis, we plotted motor RF's as opposed to visual RF's. Similar conclusions to those made in Fig. 7 were reached. Specifically, in retinotopic coordinates, motor RF's increased in area with increasing eccentricity, and the UVF RF's were smaller than the LVF RF's (**A, D**). This is consistent with Fig. 2D, E and Fig. S3. When converted to SC coordinates using the Ottes et al. model [S5] of the Robinson (1972) SC topographic map [S6], RF area was equalized in eccentricity (consistent with [S2, S5]), but the UVF/LVF asymmetry persisted (**B, E**). However, this UVF/LVF asymmetry was reduced using our amended model of Fig. 6D (**C, F**). Thus, as with visual RF's (Fig. 7), our amended model suggests that the size of the active population in the SC for a given saccade vector may be equalized in neural tissue despite changes in RF area (in retinotopic coordinates) as a function of eccentricity and UVF/LVF location. Error bars denote s.e.m.

Supplemental Experimental Procedures

LFP analyses

We sampled data at 40 KHz. The signal was first filtered in hardware (0.7-6 KHz bandwidth). We further filtered in software: we removed 50, 100, and 150 Hz line noise using an IIR notch filter and then applied a zero-phase-lag low-pass filter (300 Hz cutoff). We finally down-sampled to 1 KHz.

We analyzed filtered LFP traces like firing rates. To investigate stimulus-induced response strength, we measured peak LFP deflection 30-100 ms after stimulus onset, and we plotted it versus RF location (e.g. Fig. 5). LFP RF locations were estimated from those of nearby isolated neurons [S7]. For Fig. 5E, we binned RF locations by eccentricity (2 deg bins, with 2 deg steps) and direction (10 deg bins, with 10 deg steps). Within each bin, we plotted average stimulus-induced LFP response, after normalizing measurements within a given eccentricity bin (i.e. across all directions) by the maximum absolute value within this eccentricity bin.

Population reconstruction

We picked a stimulus location and asked how different neurons, regardless of their RF locations, responded when this stimulus was presented. This provided an estimate (in visual coordinates) of how large an SC population would be activated simultaneously for the stimulus. Naturally, neurons with RF hotspots at stimulus location were more active than other neurons. However, the breadth of the active population would depend on UVF or LVF RF areas (Fig. S4A). To include as many neurons as possible in analysis, we considered all stimuli within <3 deg from the analyzed location (e.g. from each of the locations in Fig. S4A).

For saccade-related activity (Fig. S4B), population reconstruction also allowed assessing times of peak discharge. For example, if peak saccade-related discharge for rostral neurons (i.e. neurons more foveal than the saccade endpoint) is later than peak discharge for caudal neurons (i.e. neurons representing the saccade endpoint), then this is evidence of a rostrally-directed activity spread [S2]. We should emphasize, however, that we did not explicitly record from "buildup" neurons, which show spreading most reliably [S2]. Thus, our goal was simply to demonstrate that even without explicitly searching for these neurons, our results have implications on such spreading as a function of visual field location (Fig. S4B).

SC surface topography estimates

We measured our electrode location (laterally within a recording chamber) and related it to the preferred eccentricity and direction encountered at SC surface (i.e. when the electrode tip first encountered the SC). The maximum resolution for lateral movement within a chamber was 100 μm. In depth, the electrode was movable to within 1 μm resolution as we detail below. Our recording chambers were oriented to allow orthogonal electrode penetrations of the SC for the regions that we recorded from in this structure [S8], and we confirmed this using structural MRI's. We also used guide tubes to maintain electrode straightness.

We identified SC surface using several criteria. First, we collected structural MRI's prior to implanting the monkeys, and we therefore had detailed knowledge of anatomical landmarks along the SC tracks, as well as the depth of the SC from skull surface. We used physiological correlates of anatomical landmarks, as well as electrode depth from the skull surface, to develop an estimate of where the SC should be encountered. Second, we defined SC surface as the point at which clear multi-unit activity was available, and the multi-unit activity additionally had to fit the criteria of spatially-specific visual and eye-movement related modulations. These were generally easy to see even with monkeys spontaneously scanning their environment without a specific task. Third, we had to isolate individual neurons in the same session for the session to be acceptable, and these isolated neurons had to meet all the well-known characteristics of superficial SC neurons. The average depth of the first isolated visual neuron after SC surface was 496 μm +/- 66 μm s.e.m. for monkey P and 634 μm +/- 72 μm s.e.m. for monkey N, consistent with known SC anatomy. Fourth, we confirmed (e.g. Fig. 6A), that medial electrode tracks represented upper visual field locations, lateral tracks represented lower visual field locations, rostral tracks represented central locations, and caudal tracks represented peripheral locations [S6, S9]. Finally, we confirmed that there was a known depth ordering of visual, visual-motor, and motor neurons across our penetrations. The average depth of

pure visual neurons from SC surface was 813.7 μm +/- 47.8 μm s.e.m., and the average depth of visual-motor neurons was 1290.1 μm +/- 37.5 μm s.e.m. For motor-only neurons, the average depth was 1626.1 μm +/- 227.5 μm s.e.m. These values (as well as their distributions) were remarkably similar to those reported in the literature (e.g. [S10]).

We ensured that our depth estimates reported above were accurate and repeatable by using an electrode micro-manipulator having 1 μm resolution, and we moved the electrode slowly at a speed of 1 μm/s using a computer-controlled stepper motor. We also minimized variance in our estimates of SC surface across experiments by using the following measures:

1) We fixed the electrode and manipulator to the skull of the monkey, such that the reference frame was controllable and repeatable across days.
2) We "zeroed" our electrode position in depth before every experiment (by aligning it to our skull-based reference). We did so not by hand, but by slowly moving it with 1 μm resolution using our computer-controlled micro-manipulator. The variance of our electrode "zero" position across sessions was 336 μm std. dev. for one monkey (P) and 211 μm std. dev. for the second monkey (N). As s.e.m. values, the variance values were 39.6 μm for monkey P and 30.8 μm for monkey N.
3) We regularly calibrated our micro-manipulator system, and we maintained the reference frame relative to the skull (even for guide tubes, which were mounted together with the electrodes using the same holder). This gave us consistent results in finding the SC at the depth that we expected to find it at.
4) We used structural MRI's and physiological characteristics during each penetration to predict when the SC surface should be reached relative to the skull surface. This gave us highly reliable points at which we were confident that we had hit the SC surface. To quantify this, we took all SC locations in which we visited the same SC location for two consecutive days. We had a total of 24 such unique SC locations. The mean difference in the depth of SC surface between the second and first attempts was 239.9 μm with a std. dev. of 172.4 μm.

After establishing SC surface, we instructed the monkeys to perform one of our mapping tasks described in Experimental Procedures (*delayed visually-guided saccade task* or *fixation visual RF mapping task*), and we searched for the RF hotspot. We used online (i.e. real-time) measurement and display of multi-unit activity, along with audio feedback of this activity, to find RF hotspot, and we later confirmed offline that this hotspot was similar to that obtained from the first isolated single neuron. As stated above, we sometimes visited the same electrode track location more than once. Thus, we averaged the obtained RF hotspot eccentricity and direction across the multiple visits in analyses (e.g. Fig. 6A).

Modeling

In [S5], a mapping function converts polar visual coordinates of eccentricity (R) and direction (θ) onto Cartesian coordinates (X, Y) of SC neural tissue (in mm). Neurons at X, Y are "tuned" for visual angles of R, θ according to:

$$X = B_x \log_e\left(\frac{\sqrt{R^2 + 2AR\cos(\theta) + A^2}}{A}\right) \qquad \text{(Equation S1)}$$

$$Y = B_y \arctan\left(\frac{R\sin(\theta)}{R\cos(\theta) + A}\right) \qquad \text{(Equation S2)}$$

Parameter values of A = 3 deg, B_x = 1.4 mm, and B_y = 1.8 mm provide good fits to Robinson's electrical stimulation data [S5, S6].

However, the SC contains a functional discontinuity (e.g. Figs. 2, 4, 5) across the horizontal meridian. This necessitates an over-representation of the UVF, which we confirmed (Fig. 6A, B). We thus revised the model to include a functional discontinuity:

$$X = B_x \log_e\left(\frac{\sqrt{R^2 + 2AR\cos(\theta) + A^2}}{A}\right) \qquad \text{(Equation S3)}$$

$$Y = \begin{cases} \sqrt{AF} \cdot B_y \arctan\left(\dfrac{R\sin(\theta)}{R\cos(\theta) + A}\right) & \theta > 0 \\ \dfrac{1}{\sqrt{AF}} \cdot B_y \arctan\left(\dfrac{R\sin(\theta)}{R\cos(\theta) + A}\right) & \theta \le 0 \end{cases} \qquad \text{(Equation S4)}$$

where the parameter *AF* (area factor) dictates how much the UVF representation is bigger compared to the LVF. We selected *AF* = 1.6, which seems to be in line with our experimental observations (Figs. 2, 6). This value is sufficient to roughly "equalize" the size of the active population in the SC regardless of eccentricity or UVF/LVF location (Figs. 7, S7).

Supplemental References

S1. Previc, F.H. (1990). Functional specialization in the lower and upper visual-fields in humans - its ecological origins and neurophysiological implications. Behav Brain Sci *13*, 519-575.

S2. Munoz, D.P., and Wurtz, R.H. (1995). Saccade-related activity in monkey superior colliculus. II. Spread of activity during saccades. J Neurophysiol *73*, 2334-2348.

S3. Nakahara, H., Morita, K., Wurtz, R.H., and Optican, L.M. (2006). Saccade-related spread of activity across superior colliculus may arise from asymmetry of internal connections. J Neurophysiol *96*, 765-774.

S4. Choi, W.Y., and Guitton, D. (2009). Firing patterns in superior colliculus of head-unrestrained monkey during normal and perturbed gaze saccades reveal short-latency feedback and a sluggish rostral shift in activity. J Neurosci *29*, 7166-7180.

S5. Ottes, F.P., Van Gisbergen, J.A., and Eggermont, J.J. (1986). Visuomotor fields of the superior colliculus: a quantitative model. Vision Res *26*, 857-873.

S6. Robinson, D.A. (1972). Eye movements evoked by collicular stimulation in the alert monkey. Vision Res *12*, 1795-1808.

S7. Ikeda, T., Boehnke, S.E., Marino, R.A., White, B.J., Wang, C.A., Levy, R., and Munoz, D.P. (2015). Spatio-temporal response properties of local field potentials in the primate superior colliculus. Eur J Neurosci *41*, 856-865.

S8. Chen, C.Y., Ignashchenkova, A., Thier, P., and Hafed, Z.M. (2015). Neuronal response gain enhancement prior to microsaccades. Curr Biol *25*, 2065-2074.

S9. Cynader, M., and Berman, N. (1972). Receptive-field organization of monkey superior colliculus. J Neurophysiol *35*, 187-201.

S10. Munoz, D.P., and Wurtz, R.H. (1995). Saccade-related activity in monkey superior colliculus. I. Characteristics of burst and buildup cells. J Neurophysiol *73*, 2313-2333.